Department of Applied physics

Lifetime analysis of dye and perovskite solar cells

Armi Tiihonen

Aalto University

DOCTORAL DISSERTATIONS

Aalto University publication series
DOCTORAL DISSERTATIONS 41/2018

Lifetime analysis of dye and perovskite solar cells

Armi Tiihonen

A doctoral dissertation completed for the degree of Doctor of Science (Technology) to be defended, with the permission of the Aalto University School of Science, at a public examination held at the lecture hall M1 of the school on 6th April 2018 at 12:15.

Aalto University
School of Science
Department of Applied physics
New Energy Technologies

Supervising professor
Professor Peter Lund, Aalto University, Finland

Thesis advisor
Docent Kati Miettunen, Aalto University, Finland

Preliminary examiners
Professor Helge Lemmetyinen, Tampere University of Technology, Finland
Professor Jouko Korppi-Tommola, University of Jyväskylä, Finland

Opponent
Doctor Andreas Hinsch, Fraunhofer Institute for Solar Energy Systems ISE, Germany

Aalto University publication series
DOCTORAL DISSERTATIONS 41/2018

ISBN 978-952-60-7879-3 (printed)
ISBN 978-952-60-7880-9 (pdf)
ISSN-L 1799-4934
ISSN 1799-4934 (printed)
ISSN 1799-4942 (pdf)
http://urn.fi/URN:ISBN:978-952-60-7880-9

Images: Front cover Valeriya Azovskaya, Aalto Materials platform

Unigrafia Oy
Helsinki 2018

Finland

Publication orders (printed book):
armi.tiihonen@gmail.com

441 697
Printed matter

Author
Armi Tiihonen

Name of the doctoral dissertation
Lifetime analysis of dye and perovskite solar cells

Publisher School of Science

Unit Department of Applied physics

Series Aalto University publication series DOCTORAL DISSERTATIONS 41/2018

Field of research Engineering Physics

Manuscript submitted 12 December 2017 **Date of the defence** 6 April 2018

Permission to publish granted (date) 1 February 2018 **Language** English

☐ **Monograph** ☒ **Article dissertation** ☐ **Essay dissertation**

Abstract

Dye solar cells (DSCs) and perovskite solar cells (PSCs) are promising future photovoltaics technologies. They demonstrate promise in terms of lower costs and mass-production and could thus help transform photovoltaics into a mainstream energy option. Many applications of photovoltaics, such as building integration, require a lifetime of decades to be economically sensible. This work focuses on understanding the aging mechanisms and extending the lifetime of DSCs and PSCs.

In DSCs, the insufficient stability of the electrolyte component is a major weakness. Commonly applied liquid electrolytes are difficult to seal reliably into the cell. Thus, a method for sealing large-area cells utilizing nanocellulose aerogel membranes was developed in this work. The main stability challenge is the diminution of charge carriers in electrolyte (i.e., electrolyte bleaching) when the cells are exposed to environmental stress factors. In this work, purification of electrolyte solvent was observed to halve the progress of bleaching when the cells were exposed to ultraviolet light (UV). Also the application of a UV filter and the change of the redox couple from iodine to cobalt complex effectively suppressed the bleaching. Cobalt complex electrolytes have been regarded as unstable but here it was detected for the first time that the cobalt complex bleaches at a slower rate in comparison to the traditional iodine electrolyte.

A perovskite precursor ink was developed in this work for printing carbon based PSCs. In this respect, all the material layers of the cell were manufactured accurately using upscalable methods. Perovskite decomposition under humidity or UV is a major aging mechanism. Here, the exceptionally stable PSCs prepared here were shown to withstand these stress factors in accelerated aging tests for one thousand hours. Also a photographing method was applied to explore perovskite decomposition.

A survey of the state-of-the-art degradation studies of PSCs and DSCs revealed insufficient reporting and experimental procedures. Therefore, improved procedures were elaborated upon in this work, which also could contribute to improving the lifetime of DSSC and PSC solar cells.

Keywords Photovoltaics, dye solar cells, perovskite solar cells, stability, lifetime, aging tests, electrolyte

ISBN (printed) 978-952-60-7879-3 **ISBN (pdf)** 978-952-60-7880-9

ISSN-L 1799-4934 **ISSN (printed)** 1799-4934 **ISSN (pdf)** 1799-4942

Location of publisher Helsinki **Location of printing** Helsinki **Year** 2018

Pages 167 **urn** http://urn.fi/URN:ISBN:978-952-60-7880-9

Tekijä
Armi Tiihonen

Väitöskirjan nimi
Väriaine- ja perovskiittiaurinkokennojen elinaikatutkimuksia

Julkaisija Perustieteiden korkeakoulu

Yksikkö Teknillisen fysiikan laitos

Sarja Aalto University publication series DOCTORAL DISSERTATIONS 41/2018

Tutkimusala Teknillinen fysiikka

Käsikirjoituksen pvm 12.12.2017 **Väitöspäivä** 06.04.2018

Julkaisuluvan myöntämispäivä 01.02.2018 **Kieli** Englanti

☐ **Monografia** ☒ **Artikkeliväitöskirja** ☐ **Esseeväitöskirja**

Tiivistelmä

Väriaine- ja perovskiittiaurinkokennot ovat lupaavia tulevaisuuden aurinkosähköteknologioita. Niiden avulla aurinkosähköstä voi tulla energiantuotannon valtavirtaa, kun kennot ovat nykyistä edullisempia ja helpommin teollisessa mittakaavassa valmistettavia. Monissa sovelluksissa, kuten rakennusintegraatiossa, kennoilta vaaditaan jopa vuosikymmenien elinikää, jotta investointi olisi taloudellisesti kannattava. Tässä työssä syvennytään väriaine- ja perovskiittiaurinkokennojen ikääntymismekanismien ymmärtämiseen ja eliniän kasvattamiseen.

Stabiiliuden kannalta väriainekennojen heikko lenkki on niiden elektrolyytti. Yleisesti käytettyjen nestemäisten elektrolyyttien sulkeminen kennoon luotettavasti on hankalaa, joten työssä kehitettiin tähän tarkoitukseen suurille kennoille soveltuva, nanoselluloosa-aerogeelimatriisia hyödyntävä menetelmä. Stabiiliuden päähaasteena on elektrolyytin varauksenkuljettajien väheneminen (nk. elektrolyytin vaalentuminen) ympäristön rasitteille altistettuna. Tässä työssä havaittiin, että elektrolyytin liuottimen puhdistaminen puolittaa pääasiallisen ikääntymismekanismin eli elektrolyytin vaalentumisen nopeuden ultraviolettivalolle (UV) altistetuissa kennoissa. Myös UV-suodattimen käytön sekä redox-parin vaihtamisen jodista kobolttikompleksiin havaittiin tehokkaasti hidastavan elektrolyytin vaalenemista. Työssä havaittiin ensimmäistä kertaa, että epästabiiliksi mielletty kobolttikompleksielektrolyytti vaalentuu perinteistä jodielektrolyyttiä hitaammin UV-altistuksessa.

Perovskiittikennoille kehitettiin työssä perovskiitin esiasteesta muste, joka soveltuu hiilipohjaisten kennojen valmistamiseen tulostamalla. Näin kennojen kaikki materiaalikerrokset voitiin valmistaa tarkasti laajamittaiseen tuotantoon soveltuvilla menetelmillä. Perovskiittikennoissa merkittävä ikääntymismekanismi on perovskiitin hajoaminen kosteus- tai UV-altistuksessa. Valmistettujen poikkeuksellisen stabiilien kennojen osoitettiin kestävän näitä rasitteita tuhannen tunnin kiihdytetyissä ikääntymistesteissä. Samalla tutkittiin perovskiitin hajoamista valokuvausmenetelmää käyttäen.

Työssä analysoitiin perovskiitti- ja väriainekennojen ikääntymistestien laatua viimeaikaisen kirjallisuuden perusteella. Analyysi paljasti puutteellisia kokeellisia menettelyitä sekä riittämätöntä raportointia, joten tässä työssä määriteltiin keinoja ikääntymistestien tason parantamiseen. Laadukkaammat ikääntymistestit voivat edesauttaa väriaine- ja perovskiittikennojen stabiiliuden kasvattamista tulevaisuudessa.

Avainsanat Aurinkosähkö, väriaineaurinkokennot, perovskiittiaurinkokennot, stabiilius, elinaika, ikääntymistestit, elektrolyytti

ISBN (painettu) 978-952-60-7879-3 **ISBN (pdf)** 978-952-60-7880-9

ISSN-L 1799-4934 **ISSN (painettu)** 1799-4934 **ISSN (pdf)** 1799-4942

Julkaisupaikka Helsinki **Painopaikka** Helsinki **Vuosi** 2018

Sivumäärä 167 **urn** http://urn.fi/URN:ISBN:978-952-60-7880-9

Preface

I prepared this dissertation 2013-2018 at Aalto University, Department of Applied Physics in New Energy Technologies research group. I am grateful for my opponent, doctor Andreas Hinsch, and the pre-examiners of my dissertation, professor Helge Lemmetyinen and professor Jouko Korppi-Tommola, for carefully reading my thesis.

I would like to thank these organizations for providing me with continuous funding that made my dissertation possible: Tiina and Antti Herlin Foundation, Emil Aaltonen Foundation, Aalto University Education Network in Condensed Matter and Materials Physics (CMMP), Aalto University Multidisciplinary Institute of Digitalization and Energy (MIDE, project FerroPV, 751026), the Finnish Funding Agency for Technology and Innovation (Tekes, project KesMPV, 2928/31/2010), and Academy of Finland (project SOLID, 271081). Tiina and Antti Herlin Foundation also offered grant holders useful activities, such as communications training, that provided opportunities to discuss about my research work in broader context with other grant holders and the representatives of the foundation.

I have worked in New Energy Technologies group since 2010. At that time, I started as a research assistant, preparing an automatized measurement setup for the aging tests of solar cells. Since then, I have been honored to work with people who take pleasure in progressing science and making this world a better place to live. Thank you all:

My supervisor, professor Peter Lund, whose visions for the future have inspired me in my research work and who has provided me with opportunities to attend interesting events, such as Global Young Scientists Summit. My instructor, doctor Kati Miettunen, who has tirelessly guided me with everything that a research assistant, a Master's thesis worker, and a postgraduate student has to know as a member of scientific community,

and has recognized exciting results even when they were hidden from myself in the vast piles of data. An exciting result can easily hide from the researcher herself but even more easily it hides from the public in the depths of scientific text. Thanks to doctor Janne Halme for sharing his talent to express exiting results so that they truly sound exciting. To doctor Imran Asghar for giving an example on how to continuously develop yourself — we never get ready in life. To doctor Ghufran Hashmi for introducing me with perovskite solar cells and for the inexhaustible stream of enthusiasm. To Aapo Poskela, Sakari Lepikko, and Sami Jouttijärvi for the friendly atmosphere and apt critique during our experiments, and the joint projects that have progressed smoothly. To Sini Numminen for bringing new viewpoints related to energy frugality in discussions on energy. To doctor Ying Ma and doctor Jose Raigon for interesting conversations on the duties and career of a scientist. To our research partners, doctor Jaana Vapaavuori, Sabine Rendon, doctor Denys Mavrynsky, professor Reko Leino, Gabriela Sonai, doctor Marcos Asaj, doctor Merve Özkan, and Björn Törngren for the co-operation.

A major share of the work of a physicist is to implement something planned ahead but still, the best ideas seem to arise elsewhere than in the laboratory. My thanks to Sannamari Pilpola, doctor Farid Karim, Riina Jokiranta, Alpi Rimppi, Pyry Mäkinen, doctor Kerttu Aitola, doctor Juuso Lindgren, doctor Jyri Salpakari, doctor Jani Mikkola, and all the people mentioned above for nice conversations during the coffee breaks and in the corridors, for company during the conferences, and also for fun leisure events and trips. Thanks to Antti Vepsäläinen, Jere Mäkinen, doctor Samuli Autti, Sampo Hämäläinen, and other participants for the lunches that often got stretched in the midst of conversations related to various aspects of physics spanning from the phases of He_3 to the unexpected behaviour of qubits and even to string theory.

My years as a postgraduate student have luckily involved also many other things than research. Thank you for my friends from Aalto University and Satakuntalainen Osakunta, and also back from high school, for all the get-togethers and events that have drawn my thoughts far away from the work. The retreats from work to unelectrified locations, such as our numerous hiking trips and the visits to the cottage of Satakuntalainen Osakunta at Kauvatsa village have been especially efficient. Finally, although most importantly, I thank my family, my parents Pirkko Korsimaa and Kari Tiihonen, my sister and her husband Helmi and Lauri Syrén,

and my partner Antti: your understanding and encouragement has been invaluable during all these years.

Espoo, February 23, 2018

Armi Tiihonen

Contents

Preface **1**

Contents **5**

List of Publications **7**

Author's Contribution **9**

Other publications by the author **11**

1. Introduction **13**

1.1 Overview 13

1.2 Background and scope 14

1.3 Outline of the thesis 16

2. Dye-sensitized and perovskite solar cells **17**

2.1 Dye-sensitized solar cells 17

2.2 Perovskite solar cells 19

3. Methods **23**

3.1 Aging tests 23

3.2 Key measurement techniques 24

3.2.1 Current-voltage curve measurements 24

3.2.2 Electrochemical impedance spectroscopy 26

3.2.3 Image processing technique 29

3.2.4 X-ray powder diffraction 31

4. Main results and discussion **37**

4.1 Role of impurities in the efficiency and stability of dye solar cells (Publication I and Publication II) 37

4.2 Preventing bleaching of electrolyte in dye solar cells (Publication I, Publication II, and Publication III) 43
4.2.1 Increasing the concentration of charge carriers 44
4.2.2 Initial investigations about filtering of ultra-violet light 45
4.2.3 Electrolyte purification 45
4.2.4 Chemical tailoring with hydrophobic dye 46
4.2.5 Advanced investigations about the filtering of ultra-violet light and the change of redox couple 47
4.2.6 First steps of lifetime prediction of solar cells 53
4.3 Eased assembling and more even spacial performance distribution of dye solar cells by quasi-solidifying the electrolyte (Publication IV) 55
4.4 Towards long-lived perovskite solar cells with highly reproducible performance (Publication V and Publication VI) . . . 58
4.4.1 Development of cell manufacturing technique 59
4.4.2 Perovskite solar cells durable against combined illumination and humidity 60
4.4.3 Perovskite solar cells durable against combined humidity and ultra-violet light illumination 62
4.5 Improving methodological quality of stability research of perovskite and dye solar cells (Publication VII) 64

5. Summary and conclusions **71**

References **77**

Publications **89**

List of Publications

This thesis consists of an overview and of the following publications which are referred to in the text by their Roman numerals.

I A. Tiihonen, K. Miettunen, S. Rendon, D. Mavrynsky, J. Halme, R. Leino, P.D. Lund. The effect of electrolyte purification on the performance and long-term stability of dye-sensitized solar cells. *Journal of The Electrochemical Society*, 162 (9), H661-H670 (2015).

II A. Tiihonen, K. Miettunen, S. Rendon, D. Mavrynsky, A. Poskela, M.I. Asghar, J. Halme, R. Leino, P.D. Lund. The effect of dye purification on performance and lifetime of dye-sensitized solar cells. In *29th European Photovoltaic Solar Energy Conference and Exhibition*, Amsterdam, 1513 - 1518 (2014).

III K. Miettunen, A. Poskela, A. Tiihonen, S. Rendon, K. Axenov, L. Kronberg, R. Leino, P.D. Lund. From identification of electrolyte degradation rates to lifetime estimations in dye solar cells with iodine and cobalt redox couples. *Nano Energy Systems*, 1 (2), 29-41 (2017).

IV K. Miettunen, J. Vapaavuori, A. Tiihonen, A. Poskela, P. Lahtinen, J. Halme, P.D. Lund. Nanocellulose aerogel membranes for optimal electrolyte filling in dye solar cells. *Nano Energy*, 8, 95-102 (2014).

V S.G. Hashmi, D. Martineau, X. Li, M. Özkan, A. Tiihonen, M.I. Dar, T. Sarikka, S.M. Zakeeruddin, J. Paltakari, P.D. Lund, M. Grätzel. Air processed inkjet infiltrated carbon based printed perovskite solar cells with

high stability and reproducibility. *Advanced Materials Technologies*, 2 (1), 1600183 (2017).

VI S.G. Hashmi, A. Tiihonen, D. Martineau, M. Özkan, P. Vivo, K. Kaunisto, U. Vainio, S.M. Zakeeruddin, M. Grätzel. Long term stability of air processed inkjet infiltrated carbon-based printed perovskite solar cells under intense ultra-violet light soaking. *Journal of Materials Chemistry A*, 5, 4797-4802 (2017).

VII A. Tiihonen, K. Miettunen, J. Halme, S. Lepikko, A. Poskela, P.D. Lund. Critical analysis on the quality of stability studies of perovskite and dye solar cells. *Energy & Environmental Science*, Advance Article, DOI: 10.1039/C7EE02670F (2018).

Author's Contribution

Publication I: "The effect of electrolyte purification on the performance and long-term stability of dye-sensitized solar cells"

The author is mainly responsible for this work and writing the paper, apart from developing the purification methods for cell materials.

Publication II: "The effect of dye purification on performance and lifetime of dye-sensitized solar cells"

The author is mainly responsible for this work and writing the paper, apart from the purification of cell materials.

Publication III: "From identification of electrolyte degradation rates to lifetime estimations in dye solar cells with iodine and cobalt redox couples"

The author contributed in the initial planning, experimental work, analysis of the results (including the assembling of the test cells and all the measurements apart from liquid chromatography - mass spectrometry), and writing the article.

Publication IV: "Nanocellulose aerogel membranes for optimal electrolyte filling in dye solar cells"

The author contributed to all parts of the experimental work and analysis of the results. The author took also part in writing the paper.

Publication V: "Air processed inkjet infiltrated carbon based printed perovskite solar cells with high stability and reproducibility"

The author is responsible for planning, performing, analyzing, and reporting the parts of the paper that considered the image processing of the solar cell samples. Additionally, the author took part in writing other parts of the paper. The author did not participate in the preparation of solar cells or performing the aging test apart from the image processing.

Publication VI: "Long term stability of air processed inkjet infiltrated carbon-based printed perovskite solar cells under intense ultra-violet light soaking"

The author is mainly responsible for performing the aging tests for the samples and analyzing the results of the test. The author reported the results of XRD and camera imaging measurements in the paper and took part also in writing other parts of the paper. The author did not participate in the preparation of solar cells.

Publication VII: "Critical analysis on the quality of stability studies of perovskite and dye solar cells"

The author is mainly responsible for all parts of this work and writing the paper.

Other publications by the author

Other publications by the author that are not included in the thesis.

[1] Poskela, A., Miettunen, K., Tiihonen, A., Lund, P.D. The state of external circuit affects the stability of dye-sensitized solar cells. Submitted to *Electrochimica Acta* (2017).

[2] Lepikko, S., Miettunen, K., Poskela, A., Tiihonen, A., Lund, P.D. Testing dye-sensitized solar cells in harsh northern outdoor conditions. Submitted to *Energy Science & Engineering* (2017).

[3] Törngren, B., Sandén, S., Nyman, J., Tiihonen, A., Jiang, H., Ruokolainen, J., Halme, J., Österbacka, R., Smått, J.-H. Minimizing structural deformation of gold nanorods in plasmon-enhanced dye-sensitized solar cells. *Journal of Nanoparticle Research* 19 (11), 365 (2017).

[4] Sonai, G.G., Tiihonen, A., Miettunen, K., Lund, P.D., Nogueira, A.F. Long-term stability of dye-sensitized solar cells assembled with cobalt polymer gel electrolyte. *The Journal of Physical Chemistry C* 121 (33), 17577-17585 (2017).

[5] Santana Andrade, M., Tiihonen, A., Miettunen, K., Lund, P.D., Nogueira, A.F., Pastore, H.O. Gel electrolytes with polyamidopyridine dendron modified talc for dye-sensitized solar cells. *ACS Applied Materials & Interfaces* 9 (24), 20454-20466 (2017). DOI: 10.1021/acsami.7b00897

[6] Santana Andrade, M., Miettunen, K., Tiihonen, A., Lund, P.D., Nogueira, A.F., Pastore, H.O. Stabilizing dendron-modified talc-based electrolyte for quasi-solid dye-sensitized solar cell. *Electrochimica Acta* 228, 413 - 421 (2017). DOI: 10.1016/j.electacta.2017.01.101

[7] Santana Andrade, M.A., Nogueira, A.F., Miettunen, K., Tiihonen, A., Lund, P.D., Pastore, H.O. Quasi-solid electrolyte with polyamideamine dendron modified-talc for dye-sensitized solar cells. *Journal of Power Sources* 325, 161-170 (2016). DOI: 10.1016/j.jpowsour.2016.06.041

[8] G.G. Sonai, A. Tiihonen, K. Miettunen, P.D. Lund, A.F. Nogueira. Preventing UV degradation in dye-sensitized solar cells. In *32nd European Photovoltaic Solar Energy Conference and Exhibition*, Munich, 1347 - 1352 (2016). DOI: 10.4229/EUPVSEC20162016-3DV.2.55

[9] M. Özkan, S.G. Hashmi, M. Borghei, A. Tiihonen, K. Lobato, A.F. da Cunha, O.J. Rojas, P.D. Lund, J. Paltakari. Highly transparent cellulose substrate for dye sensitized solar cells. In *32nd European Photovoltaic Solar Energy Conference and Exhibition*, Munich, 1353 - 1356 (2016). DOI: 10.4229/EUPVSEC20162016-3DV.2.56

[10] Rendon, S.M.K., Mavrynsky, D., Meierjohann, A., Tiihonen, A., Miettunen, K., Asghar, I., Halme, J., Kronberg, L., Leino, R. Analysis of dye degradation products and assessment of the dye purity in dye-sensitized solar cells. *Rapid Communications in Mass Spectrometry* 29, 1-7 (2015). DOI: 10.1002/rcm.7384

[11] Miettunen, K., Saukkonen, T., Li, X., Law, C.H., Sheng, Y.K., Halme, J., Tiihonen, A., Barnes, P.R.F., Ghaddar, T., Asghar, I., Lund, P.D., O'Regan, B.C. Do counter electrodes on metal substrates work with cobalt complex based electrolyte in dye sensitized solar cells?, *Journal of the Electrochemical Society* 160 (2), H132-H137 (2013). DOI: 10.1149/2.074302jes

[12] Asghar, M. I., Kaukonen, S., Tiihonen, A., Vahlman, H., Halme, J., Lund, P.D. Application of image processing method to investigate stability of different kinds of counter electrodes for dye solar cells. In *28th European Photovoltaic Solar Energy Conference and Exhibition*, 2796-2798 (2013). DOI: 10.4229/28thEUPVSEC2013-3DV.2.47

1. Introduction

1.1 Overview

Energy production must be modernized in the decades to come. More secure and sustainable energy production techniques are needed because conventional easily available fossil-fuels are limited in the long-term, particularly when considering increasing future energy demands and especially with reference to emerging economies. Climate change is another well-known driver for the development of new energy production technologies as it is currently among the greatest environmental and societal challenges facing humankind.

The Paris Climate Agreement, signed by 197 countries in 2015 and ratified by 166 countries to date, pursues limiting the global temperature increase to less than 1.5°C compared to the pre-industrial level [1]. Constraining global warming to this limit is believed to significantly reduce the risks and impacts of climate change [1]. Reaching this ambitious target requires a rapid decrease in greenhouse gas emissions globally, 60% of which arises from energy production [2].

Therefore, increasing the share of renewable energy in energy production is an effective way for limiting the emissions. The share of renewable energy, such as hydroelectric, wind, solar, and bioenergy, in global energy production is still rather low: 13.4% of the primary energy and 22.8% of electricity production in 2015 [3]. However, the recent increase is remarkable: approximately 50% between 2010 and 2015 [4]. The efforts on application and research of renewable energy are further accelerated now that the Paris Climate Agreement has been reached.

In particular, photovoltaics (PV) have a massive potential; in principle the whole energy demand of humankind could be produced solely with PV

[5]. In 2016, the global installed solar PV capacity accounted for 306.5GW [6] which corresponds to roughly 1.8% of the global electricity demand [7]. The greatness of this value might be a matter of opinion but the growth rates are undeniably impressive: The average annual growth rate of PV between 1990 and 2015 is more than 45% [3]. Furthermore, 2016 was a record year with the largest ever global installation of solar PV capacity (with an increase of 50% from 2015) [6]. Grid parity has already been approached (or will soon be approached) in many parts of the world such as in Europe, which will accelerate installations in the near future.

Third-generation solar cell technologies are being developed to overcome these challenges and provide even more affordable and sustainable electricity. In this work, the focus has been on two of them: dye-sensitized and perovskite solar cells. Both cell types can be manufactured from low-cost materials using energy-efficient methods that are suitable for large-scale production [8, 5], such as roll-to-roll methods. They can be produced from a variety of active material and substrate combinations, resulting in different colors, transparency, and even flexibility [9, 10, 11]. These properties could suppress the production cost and expand the application area of PV. For instance, building-integrated PV could be applied to a larger scale [12, 13] and with more architectural variety in the future [9].

The energy-conversion efficiencies of both cell types are sufficient for applications (record for dye solar cells $11.9\pm0.4\%$ and for perovskite solar cells $19.7\pm0.6\%$ [14, 15]) if the production costs are low enough. However, the lifetime and durability of the cells is to date insufficient [16, 12] for most applications. Additionally, efficient energy production requires that the lifetime of the cells should be significantly longer than the energy payback time of the devices in order to use the devices efficiently for energy production. Thus, further research on the stability of these devices is essential for the large-scale commercialization of these devices.

1.2 Background and scope

This thesis concentrates on understanding the mechanisms affecting the stability of dye-sensitized and perovskite solar cells and developing methods for increasing the lifetime of the cells. The focus is on preventing the degradation of electrolyte in dye solar cells and the decomposition of perovskite in perovskite solar cells.

Since both degradation paths are strongly linked to environmental stress

factors activating the degradation, special attention has been given to the effects of environmental conditions on the lifetime of the cells, specifically visible light, ultra-violet light, and air humidity. Stability research relies strongly on experimental aging tests of devices. Thus, also the methodological quality of aging tests in the field was analyzed and suggestions developed for improving the effectivity of aging testing in future.

The successful operation of dye solar cells relies on the energy level compatibility of the materials in the cells, and the long-term stability of the devices requires that the chain of chemical reactions leading to the energy conversion remains flawless during the millions of repetitions during the lifetime of the cell. Thus, even small concentrations of impurities could distract the operation of the cells, leading to degradation. The role of impurities and purification of the two dye solar cell components, dye and electrolyte (including the individual compounds of the electrolyte), were investigated in this thesis.

Degradation of electrolyte is a major stability challenge of dye solar cells [17]. In many cases, the degradation proceeds mainly via the loss of charge carriers in electrolyte, i.e., electrolyte bleaching [17]. Thus, several methods for preventing or suppressing electrolyte bleaching were explored in this thesis. The focus here was on electrolyte bleaching triggered by the exposure to ultra-violet light illumination. The dominance of electrolyte bleaching in the degradation of the investigated dye solar cells also created an opportunity to take initial steps for predicting the lifetime of the cells by measuring the progress of the main degradation mechanism.

Best efficiencies and longest lifetimes of dye solar cells are both recorded with liquid electrolytes [8] but the effective sealing of liquid electrolyte into the dye solar cell is challenging. Additionally, many typical sealing methods of liquid electrolytes are not optimal for large-scale production [18, 19, 20, 21]. Quasi-solid electrolytes could make the sealing process easier and thus prevent leakages. Therefore, a method applicable in large scale production for creating a quasi-solid electrolyte from an operational liquid electrolyte was developed in this work, utilizing a nanocellulose aerogel membrane.

Most perovskite solar cell architectures presented in the literature require manual work which is not applicable in large scale production and could act as a source of increased variations in the performance of the prepared cells. In this work, a truly upscalable method for preparing printable hole-transporting material free carbon based perovskite solar cells

was developed. The key step was the development of perovskite precursor ink that is applicable for this cell type. Perovskite solar cells are typically regarded as rather unstable devices in which degradation can proceed, e.g., via perovskite decomposition [22]. As in the case of dye solar cells, the degradation could be triggered by multiple different causes such as environmental stress factors or the combination of cell materials [16, 22]. Thus the long-term stability of the fabricated, exceptionally stable devices was investigated by exposing cells to visible light, ultra-violet light, and humidity. In particular, the signs of possible decomposition of perovskite were sought, and also an image processing technique was applied for the tracking of perovskite decomposition.

The stability research of dye and perovskite solar cells relies on aging tests. The test results depend greatly on the values of the environmental variables during the test because they can activate different aging mechanisms, resulting in completely different results from the test. Additionally, the aging tests are typically long, resulting in the accumulation of nuisance factors in the test results. Therefore, gaining consistent and useful information from the aging tests requires wide knowledge on the aging mechanisms of the cells in addition to the nuisance factors of the tests. In this work, the methodological quality of recent aging tests of perovskite and dye solar cells was analyzed based on a wide literature investigation and alarming deficiencies were found. Based on the results, methods for improving the quality of aging tests were suggested.

1.3 Outline of the thesis

This thesis is based on the seven original publications listed in the List of Publications and divided into five chapters. In Chapter 1, the overview and the background as well as the outline of the thesis are given. The principles of dye solar cells and perovskite solar cells are presented in Chapter 2. The experimental methods, i.e. aging tests and focal measurements techniques combined with the aging tests in this thesis, are introduced in Chapter 3. Chapter 4 presents and discusses the main results, and finally Chapter 5 summarizes the conclusions of this thesis.

2. Dye-sensitized and perovskite solar cells

Dye-sensitized solar cells (DSCs) and perovskite solar cells (PSCs) are electrochemical photovoltaic devices converting light to electricity. Both devices are based on similar operating principles although the implementation is different.

2.1 Dye-sensitized solar cells

A schematic structure of a typical DSC is illustrated in Fig. 2.1a. Operational DSCs can be assembled from a great variety of material options but all consist of three main components: a photoelectrode (PE), a counter electrode (CE), and an electrolyte. PE consists of a semiconductor layered on top of a conducting substrate and dyed using a suitable dye. The semiconductor layer is typically nanoporous, which is a necessity in gaining good efficiencies because compared to a compact layer, the nanoporous layer offers approximately a 1,000 times greater absorption area for the dye. The electrolyte, which includes a redox couple and fills the space between the PE and CE, is typically also absorbed in the nanoporous semiconductor layer. CE consists of a conducting substrate and a catalyst layer that facilitates the operation of the redox couple. The electrons generated in the cell are channeled to the external electric circuit using electric contacts attached to both substrates. To allow the absorption of light in the cell, at least one of the substrates must transmit light. DSCs are typically sealed from the edges using, for instance, thermoplastic or glass frit sealing to prevent electrolyte (that is commonly liquid) from leaking or evaporating out from the cell and impurities from entering the cell.

The operation of an illuminated DSC illustrated in Fig. 2.1b is based on the compatibility of the energy levels of the materials. A photon is absorbed by the dye with light-harvesting efficiency η_{LH}, resulting in the

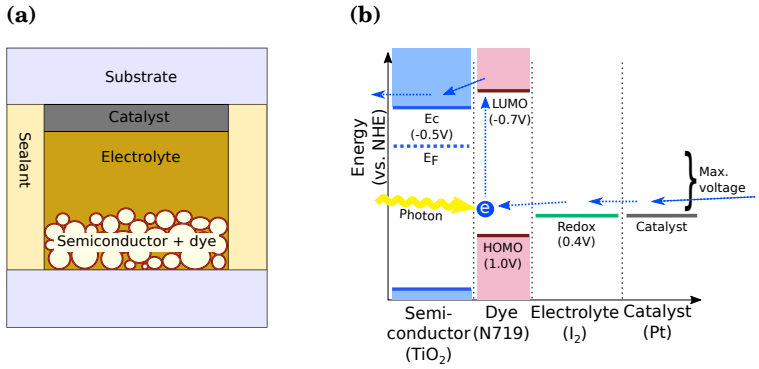

Figure 2.1. a) Structure and b) energy level schematics of a typical dye solar cell. Constructed based on [23, 24].

excitation of an electron to a higher energy state (from the highest occupied molecular orbital, HOMO, to the lowest unoccupied molecular orbital, LUMO). The photons are not absorbed by the semiconductor because its band gap is too large to allow excitations by visible light. The LUMO level of the dye is higher than the conduction band of the semiconductor and the contact between the dye and the semiconductor nanoparticles is strong, so the electron transfers from the dye to the conduction band of the semiconductor. The efficiency of the process is the injection efficiency η_{INJ}. In the semiconductor, the electron is diffused to the conducting substrate and, finally, to the external circuit, with collection efficiency η_{COL}. Simultaneously, the oxidized dye is recovered (with regeneration efficiency η_{REG}) by receiving an electron from the redox couple of the electrolyte because the redox energy level is higher than the HOMO level of the dye. The concentration of the oxidized redox couple ions is higher close to PE when the cell is illuminated. Thus, the oxidized ion diffuses towards the CE where it is reduced back to the original state by accepting an electron coming from the external circuit in a reaction catalyzed by the catalyst. The loop is then closed and, ideally, no chemical transformations remain in the cell.

In reality, multiple loss mechanisms exist. The two major loss mechanisms in a typical DSC involve the charge recombination of the excited electron from the LUMO level to the ground state of the dye, and the recombination of the injected electrons to redox ions [25] (called dark current in this work). Electrons could also transfer from the semiconductor conduction band to the dye ground state (although the reaction is hindered because it lies at the Marcus inverted region [26]), or leak from the

conducting PE substrate to the electrolyte (which can be suppressed, e.g., by using a compact metal oxide blocking layer).

The output current of the cell is determined by reaction efficiencies η_{LH}, η_{INJ}, η_{COL}, and η_{REG} [23, 27, 26]. The maximum output voltage is the difference of the quasi-Fermi level of the semiconductor and the redox level [25]. A high-quality DSC is designed to minimize the losses and maximize the generated electric power. η_{LH} is increased if the HOMO and LUMO levels are close to each other because then the dye absorbs lower energy photons. The LUMO level should still remain higher than the conduction band of the semiconductor, otherwise the driving force of the injection is poor and excited electrons recombine back to the ground state of the dye (η_{INJ} decreases). η_{COL} is maximized by designing the dye so that it covers the semiconductor surface efficiently (hindering dark current), ensuring a good contact between the semiconductor nanoparticles, using a not overly thick semiconductor layer, and applying a suitable blocking layer between the substrate and semiconductor layer to suppress the recombination from the substrate to the electrolyte. The redox level of the electrolyte should be low to maximize the maximum voltage of the cell but remain higher than the ground state of the dye to facilitate η_{REG}. The alterations of energy levels and reaction rates are in practice achieved, for example, through additive materials such as tert-butylpyridine, or by the tailoring of the molecules.

Undesired reactions of the cell materials can also cause permanent changes that degrade the performance of the cell in time. There are a variety of such reactions depending on the cell configuration, and they could be activated by certain stress factors. Some examples of degradation mechanisms are the decomposition of dye, desorption of dye from the semiconductor layer, corrosion at CE, or loss of charge carriers in electrolyte. The loss of charge carriers in electrolyte is in this work called electrolyte bleaching regardless of the possible visual color change in the electrolyte. Bleaching is the dominating degradation mechanism of DSCs in all the articles exploring the degradation mechanisms of DSCs in this thesis.

2.2 Perovskite solar cells

Perovskite is the key in the operation of PSCs. The term "perovskite" has many meanings. In the context of PSCs, it refers to a wide group of hybrid inorganic-organic materials with perovskite crystal structure which can

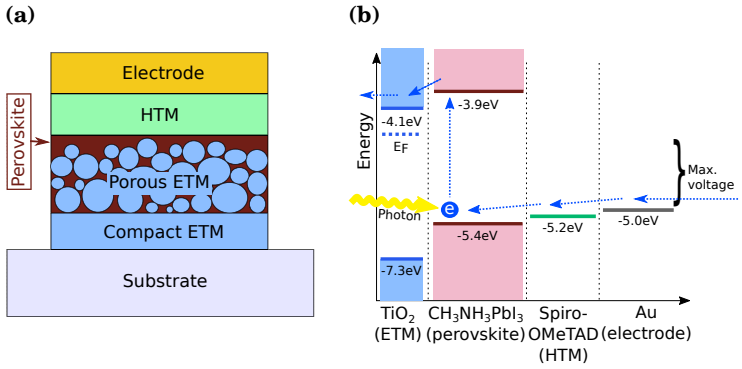

Figure 2.2. a) Structure and b) energy level schematics of a traditional mesoscopic perovskite solar cell. The values of the energy levels are adopted from [31].

be used as a light harvester in PSCs, e.g., methylammonium lead halides.

The very first perovskite solar cells were traditional DSCs in which perovskite was used as a dye [28]. Later, the electrolyte in the DSC configuration was replaced with a hole-transporting material (HTM) [29, 30] and a mesoscopic PSC, illustrated in Fig. 2.2a was created: Perovskite crystals are formed inside the nanoporous electron transporting material (ETM) layer (e.g., TiO_2) that has been prepared on the supporting conducting substrate. These layers are topped with a HTM (e.g., 2,2,7,7-tetrakis-(N,N-di-p-methoxyphenylamine)9,9-bifluorene i.e. spiro-OMeTAD) layer and a hole extracting electrode. PSCs need only one supporting substrate, unlike DSCs that typically require two supporting substrates. However, a supporting or protecting layer is sometimes placed on top of the operational PSC layers to increase the lifetime and durability of the cell.

The detailed operation of PSCs is still under discussion [32], but the main principles illustrated in Fig. 2.2b are commonly agreed: Incoming light is absorbed by the perovskite and the excited electrons are transferred from the conduction band of the perovskite to the conduction band of the ETM, and diffused to the external circuit. The holes created in the process are transferred into the HTM layer and diffused to the hole extracting electrode where they recombine with the electron arriving from the external circuit.

Loss mechanisms decreasing the performance of PSCs result from electrons and holes recombining at a wrong place, such as in the perovskite, between the ETM and HTM, or between the ETM and perovskite. Efficiency can be increased by additives or additional layers that enhance the charge separation and prevent premature recombination. The perfor-

mance of the cells is optimized also by selecting and engineering the materials to achieve better energy level compatibility. For example, the band structure of the perovskite can be fine-tuned by doping the perovskite [33].

The efficiency record of small PSCs has rapidly increased: from 3.8% (2009, [28]) of the first published operational PSCs to the independently confirmed value of 19.7$\pm$0.6% (2015, [14, 15]. The current efficiency record, 22.1%, has been reached using the mesoporous cell configuration [33]. Typically, PSCs with the highest efficiencies show poor stability [16]. One reason for the suppressing of the lifetime of traditional PSCs is the instability of the applied HTM materials that is caused by degradation mechanisms like halide and metal ion migration [34, 22]. Additionally, the best-performing HTM materials are costly [34].

Perovskites have been detected to be capable of playing the roles of a light harvester and hole transporter [35, 36, 37], which has resulted in another PSC configuration, a HTM free PSC. The simplified device structure has been expected and proven to result in more stable devices than by using the traditional structure [34]. However, the efficiencies lag behind the traditional cell structure [34].

The PSCs investigated in this thesis are HTM-free devices with a hole-extracting electrode made of carbon. Carbon has potential as electron extracting electrode material because it is affordable (unlike for instance Au), stable, and water-repellent [34, 38]. Water is one of the most severe stability issues of PSCs [32] and it has been detected to cause degradation via multiple routes such as the decomposition of HTM (e.g. spiroOMeTAD) and, perhaps most importantly, perovskite [39, 40, 38, 16].

The structure of carbon PSCs in this thesis is illustrated in Fig. 2.3a. Four layers are printed on top of a transparent conducting substrate: compact TiO_2 and nanoporous TiO_2, ZrO_2, and carbon. The nanoporous layers are infiltrated with perovskite precursor solution forming methylammonium lead iodide crystals in the cell.

The operation of HTM-free carbon based PSCs is shown in Fig. 2.3b.The incoming light excites electrons to the conduction band of the perovskite. The electrons are injected to the conduction band of TiO_2 that serves as an electron transporter, and diffused out from the cell. The ZrO_2 that has a large bandgap and the conduction band energy clearly different from the conduction band energy of the TiO_2, hinders the access of the excited electrons to the hole extracting electrode [41], which improves the performance of the cell. The formed holes shift into the carbon layer because of

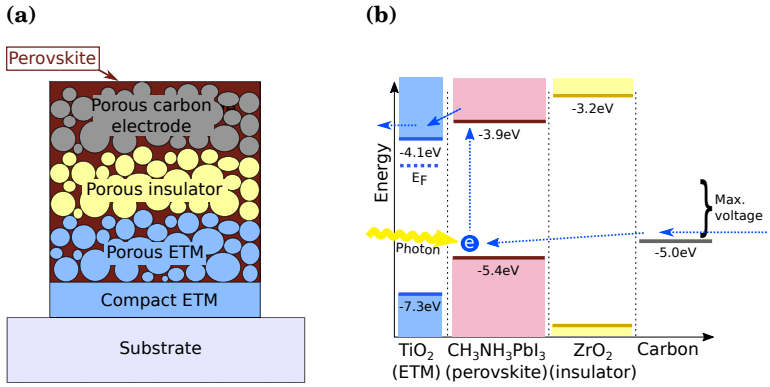

Figure 2.3. a) Structure and b) energy level schematics of a hole-transporting material free carbon based perovskite solar cell. The values of the energy levels are adopted from [42, 41, 34].

the favourable energy level alignment of the materials, and the compact layer of TiO_2 that does not adsorb the perovskite precursor prevents the direct access of the holes to the electron extracting electrode. The output current of the cell is formed of the electrons reaching the electron extracting electrode, and the maximum output voltage is the difference between the quasi-Fermi levels of the TiO_2 and carbon.

3. Methods

3.1 Aging tests

Aging tests of DSCs and PSCs are the experimental basis of this thesis. The details of the test conditions vary from one article to another depending on the motivation of the study, but the main principles are described here.

An aging test is performed for selected groups of solar cells. One of the cell groups is typically a reference group. It is either formed of cells similar to the other test groups but is kept under reference conditions during the aging test (e.g., other groups are aged under illumination and the reference group is stored in the dark), or it is formed of a different cell type and aged under similar conditions than the other groups (e.g., an established cell type with relatively well known stability vs. cells with new materials). The reference allows for detecting unexpected flaws in the methodology or the implementation of the aging test.

The test conditions are selected based on the aims of each study. All the aging tests in this thesis are illuminated ones. A typically applied reference spectrum for solar cells is AM1.5G spectrum (defined in ASTM G173 standard) that corresponds to the solar irradiation on Earth when the angle of the Sun is 37° from zenith and has an intensity of 1,000W/m^2 (i.e., 1Sun intensity). In practice, this spectrum is not achieved but other spectra with the same intensity resembling AM1.5G are applied. In the aging tests included in this work, three different illumination spectra with approximately 1,000W/m^2 intensity have been utilized: A) halogen lamps (Philips 13117), B) halogen lamps (Philips 13117) combined with either 390nm or 400nm UV light filter, or C) mercury lamps (Osram Ultra-Vitalux 300W UV+visible). They are illustrated in Fig. 3.1.

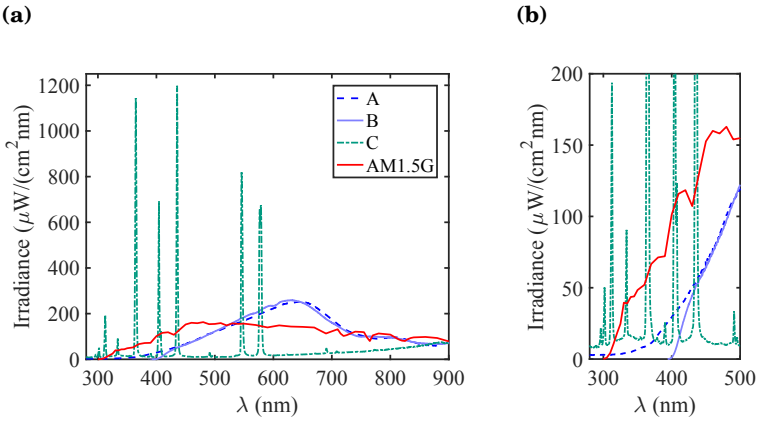

Figure 3.1. a) Illumination spectra A-C applied in the aging tests included in this thesis and AM1.5G spectrum, and b) a magnification of the spectra at 400nm cut-off wavelength of the UV filter applied in spectrum B. The spectra have been measured with spectroradiometer Ocean Optics USB2000+.

All the tests have been performed in ambient indoor air. The illumination has increased the temperature of the cells to approximately 40°C and the exact temperature has been defined in each publication. In this kind of heated setup, typical relative air humidity is approximately 45% but the exact value has been defined in the publications when it has been measured. Seasonal air humidities vary greatly.

Two different electrical states have been applied in the aging tests included in this study: the cells have either been aged at open circuit or connected to an in-house built aging test system, SCATU, and in both cases frequently (e.g., weekly) removed from the aging device for manual measurements. In SCATU, the current-voltage curve (see Section 3.2.1) and/or electrochemical impedance spectroscopy (see Section 3.2.2) are continuously measured from the cells one by one according to the sequence programmed to SCATU, and between the measurements the cells remain at open circuit.

3.2 Key measurement techniques

3.2.1 Current-voltage curve measurements

Current-voltage (IV) curve, an example of which is presented in Fig. 3.2, is the basis of the analysis of solar cells. IV curve is obtained by measuring the current of a solar cell as a function of the voltage applied to the cell.

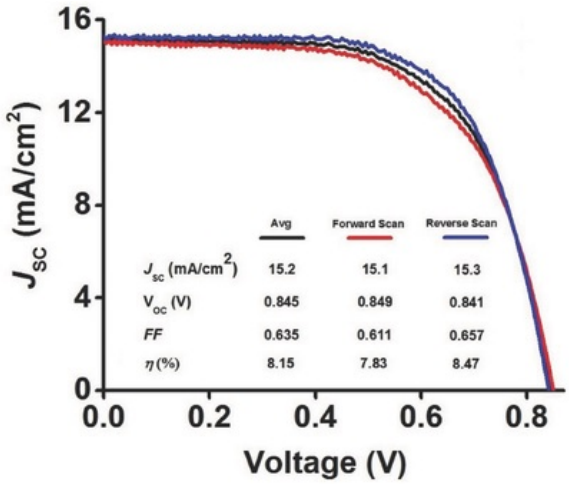

Figure 3.2. IV curve of a perovskite solar cell under 1Sun illumination. Reprinted from Publication V with permission.

Typically, a two-way sweep is applied to detect possible hysteresis that could result from a sweep that is too fast and does not allow the cell to stabilize in between the measurement points.

The basic parameters describing the performance of a solar cell are short circuit current density I_{sc}, open circuit voltage V_{oc}, fill factor FF, and efficiency η. They are calculated from an IV curve:

$$I_{\mathrm{sc}} = I(V = 0), \tag{3.1}$$

$$V_{\mathrm{oc}} = V(I = 0), \tag{3.2}$$

$$FF = \frac{P_{\mathrm{max}}}{I_{\mathrm{sc}} V_{\mathrm{oc}}}, \tag{3.3}$$

$$\eta = \frac{P_{\mathrm{max}}}{P_{\mathrm{in}}} \tag{3.4}$$

where P_{max} is the maximum output power density of the cell and V_{mpp} and I_{mpp} are the voltage and current density of the cell at the maximum power point, respectively.

The form of an IV curve depends on the environmental conditions under which it has been measured. Therefore, standard reporting conditions have been agreed for determining the efficiency of the cell: an illumination spectrum called Air Mass 1.5G (AM1.5G), P_{in} of 1,000 Wm^{-2} and temperature of 25°C [43]. These are referred to in the abbreviated form of 1Sun conditions. AM1.5G spectrum cannot be achieved completely but typically other spectra close to it, for instance giving the same amount of photons in the photoactive region, are applied.

IV curve measurements are utilized not only for determining the efficiency but also for investigating the operation of the cell. In this thesis, IV curves measured as a function of light intensity have been used for determining the limiting current density of the cell, I_{lim}, arising from mass-transport limitations. In the case of DSCs, dye molecules oxidized under illumination are recovered by electrolyte redox couple, that is recovered at CE. At high current densities, the current generation actually starts to be limited by the diffusion of redox couple molecules because dye molecules are not regenerated quickly enough. For instance for iodine redox couple, the species limiting the mass transport in electrolyte is tri-iodide, I_3^-, and

$$I_{\mathrm{lim}} = \frac{4FD_{\mathrm{I}_3^-}C^*_{\mathrm{I}_3^-}}{d_{\mathrm{el}}}, \tag{3.5}$$

where F is the Faraday's constant, $D_{\mathrm{I}_3^-}$ is the diffusion coefficient of I_3^-, $C^*_{\mathrm{I}_3^-}$ is the equilibrium electrode surface concentration of I_3^-, and d_{el} is the distance between the electrodes(that are assumed planar instead of porous in this equation) [23].

I_{sc} of a typical cell is almost linearly dependent on P_{in} over a scale of P_{in}. Excluding major resistive losses, the relation is only broken when the maximum current generation capability of the cell is met at a high enough P_{in}. From that point on, I_{sc} approximately stabilizes to I_{lim}. Eq. (3.5) illustrates that I_{lim} is a function of the concentration of the limiting charge carrier species. Thus, IV curves measured as a function of light intensity before and after the aging test can be used for analyzing the possible elecrolyte degradation arising from the depletion of charge carriers in the electrolyte. I_{lim} can also be measured by applying a voltage over the cell (instead of illumination P_{in}) but that might require a large bias which could in turn, in some cases, result in anomalous chemical reactions in the electrolyte.

Also the degradation of PE during the aging test can be detected: in a typical case, the degradation of the photoelectrode (e.g., reduced efficiency of transforming the absorbed photons to free electrons) results in the decrease of I_{sc} under any illumination intensity instead of only higher intensities like in the case of decreased I_{lim}.

3.2.2 Electrochemical impedance spectroscopy

Electrochemical impedance spectroscopy (EIS) gives detailed information about the resistance and capacitance of the components of the solar cell [23]. In EIS, voltage V consisting of a direct component V_{DC} and a sinu-

soidal component $V_{\mathrm{AC}}(\omega, t)$ alternating with angular frequency ω in time t, is applied to the solar cell and the resulting current $i_{\mathrm{AC}}(t)$ is measured. The impedance of the cell Z is:

$$Z = \frac{V_{\mathrm{AC}}(\omega, t)}{i_{\mathrm{AC}}(\omega, t, V_{\mathrm{DC}})}. \tag{3.6}$$

EIS data is collected by sweeping through a spectrum of ω. Additionally, the EIS result is affected by the internal electric state of the cell, which in turn is affected by the environment (e.g., illumination or temperature). Usually, the values of V_{DC} are selected between 0V and V_{oc} of the cell because the values of Z inside the actual operation regime of the cell are typically of interest. The amplitude of V_{AC} is small, e.g., 10mV, to avoid deviating the cell too much from the equilibrium so that the measured resistances could be assumed constant in the tested voltage region.

EIS result in which the impedance of the cell consists of real and imaginary parts Z' and Z'', respectively, is typically presented as three separate plots: $Z''(Z')$ (a Nyquist plot), $Z'(\omega)$, and $Z''(\omega)$. EIS is applied in solar cell research because the different components of the cell have different characteristic frequencies in the case of many solar cell configurations. As a result, the cell components create distinguishable arcs and peaks in Nyquist plot and frequency plots, respectively. This provides a possibility to investigate the resistance and capacitance arising from individual cell components instead of just the values of the complete cell.

The width of the arc in Nyquist plot is equal to the series connected resistance that arises from the corresponding cell component. The total series connected resistance of the cell is the sum of the resistances arising from the individual cell components and the Ohmic series resistance of the cell, R_s.

In this thesis, EIS analysis is applied only for DSCs because connecting EIS to the physics of PSCs is still under research [44]. An exemplary EIS data of a DSC is presented in Fig. 3.3. Typically, the arcs arising from PE, electrolyte, and CE of the cell are separated in the Nyquist plot of a DSC. Each arc is associated with the cell component experimentally by assembling cells with different configurations (such as CE-CE cells in order to produce EIS data with missing PE arc). In a typical DSC, CE is visible in the kHz region, PE around 1-10Hz, and the electrolyte around 0.01-1Hz [23].

EIS data is further analyzed by fitting a suitable equivalent circuit of a solar cell to the data. In this thesis, a circuit described in detail in the literature [23] has been applied. The resistance of charge transport in

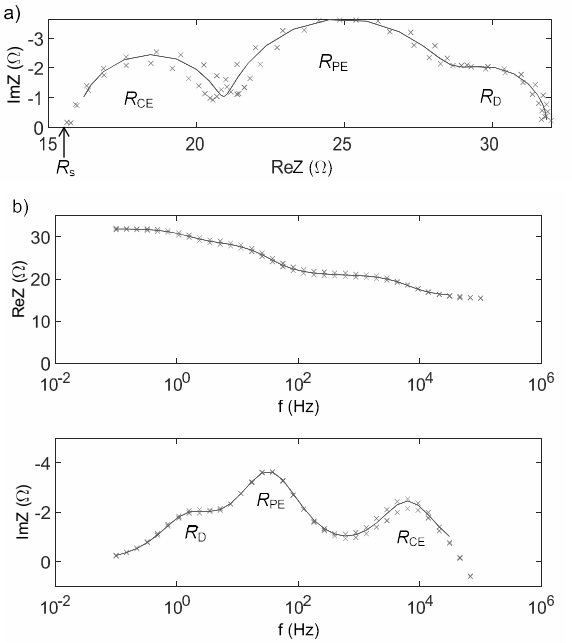

Figure 3.3. Typical electrochemical impedance spectroscopy results of a dye solar cell as a) a Nyquist curve and b) frequency spectra. The elements marked on the graph are related to the series resistance (R_s), photoelectrode (R_{PE}), counter electrode (R_{CE}), and electrolyte (R_{D}) of a DSC. The cross marks represent the measured data and the solid lines are the fit results. A derivative from Publication I supplementary data under CC-BY license.

cell materials or at the interfaces between the cell components is represented in the model by resistive components and the charge accumulation at the interfaces is represented by capacitive components: electron transport resistance of $\mathrm{TiO_2}$ film (R_T); charge recombination resistance including also the dark current (R_{REC}); PE capacitance (C_μ); contact resistance (R_{CO}) and capacitance (C_{CO}); charge transfer resistance and capacitance between the substrate and the electrolyte (R_{SU} and C_{SU}, correspondingly); charge transfer resistance and capacitance at the interface between CE and electrolyte (R_{CE} and C_{CE}, correspondingly); mass transport impedance at CE due to ionic diffusion in the electrolyte; (Z_D), and series resistance of the cell R_s.

The selected equivalent circuit model for DSCs is very comprehensive but the number of variables is so large that the fitting of the equivalent circuit to the data is challenging. Thus, the model is simplified by combining the first three components related to PE together and assuming good-quality substrates ($R_{\mathrm{SU}} \rightarrow \infty$ and C_{SU}=0) and contacts (R_{CO}=0 and C_{CO}=0). As a result, only six components remain: R_{PE} and C_{PE}, R_{CE} and

C_{CE}, R_s and R_D that is the steady state value of Z_D [23]. In reality, the RC-circuits are not ideal in solar cells which is compensated for by replacing the capacitances with constant phase elements (CPE) that bring in an additional fit parameter for each CPE, namely the ideality factor [45].

The assumptions of the model should be met during the EIS measurement to accumulate meaningful data. Additionally, the parameters of the model should remain approximately constant during the EIS measurement to acquire meaningful data. As a result, not all the model parameters can be investigated based on the same EIS measurement. R_{CE} and R_{D} should be measured at V_{oc} because both are functions of the current through the cells, I_{cell} [23]. E.g., for a DSC containing iodine electrolyte with iodine redox couple $\mathrm{I_3^-}$-$\mathrm{I^-}$:

$$R_D = \frac{k_B T}{2q}\left(\frac{1}{I_{\mathrm{lim,I_3^-}} - I_{\mathrm{cell}}} + \frac{3}{I_{\mathrm{lim,I^-}} + I_{\mathrm{cell}}}\right) \tag{3.7}$$

where $I_{\mathrm{lim,I_3^-}}$ and $I_{\mathrm{lim,I^-}}$ are the limiting current densities of $\mathrm{I_3^-}$ and $\mathrm{I^-}$, respectively (see Eq. (3.5) for $I_{\mathrm{lim,I_3^-}}$) [23]. PE is at a steady state when the recombination current at PE is small, i.e., in the dark [23].

It should be noted that at zero polarization the charge transfer resistance at the interface between CE and electrolyte is

$$R_{\mathrm{CE},0} = \frac{k_B T}{2Fkc_{\mathrm{I_3^-},eq}^{1-\beta/2} c_{\mathrm{I^-},eq}^{\beta/2}} \tag{3.8}$$

where k_B is Boltzmann constant, T is temperature, F is Faraday's constant, k is the rate constant for the charge transfer reaction at the counter electrode, $c_{\mathrm{I_3^-},eq}$ is tri-iodide equilibrium concentration, $c_{\mathrm{I^-},eq}$ is iodide equilibrium concentration and β is a symmetry parameter depending on the catalyst [23]. The equation shows that $R_{\mathrm{CE},0}$ is dependent on the concentrations of the redox couple in the electrolyte, i.e., R_{CE} depends not only on the counter electrode properties but also on the electrolyte properties. Thus it is not possible to determine if the changes in R_{CE} result from changes in counter electrode or electrolyte, or both, based solely on EIS.

3.2.3 Image processing technique

Image processing is a non-destructive method for following the degradation of solar cells. It was originally developed for investigating the degradation of the electrolyte in DSCs [46] but in this thesis it is shown to be applicable also for inspecting the degradation of PSC via perovskite decomposition.

Many cell degradation mechanisms change the appearance of the cell. Desorption of red dye results in a red hue of the electrolyte (because the dye molecules are released to the electrolyte), decomposition of the dye could result in the faded color of the cell, the loss of charge carriers in the electrolyte can change the color of the electrolyte (in the case that the color of the charge carrier compound is different from the color of the degradation result), and decomposition of dark brown perovskite leads to the appearance of bright yellow lead iodide, PbI_2. Although the appearance of the cell changes, all but severe degradation is hard to detect using only the eye because the time scale of an aging test is typically long, ranging from dozens to thousands of hours, and the changes occur very gradually. Additionally, the observation remains at a qualitative level even if the degradation is noticeable.

The image processing technique facilitates the detection of color changes and can provide quantitative data about the degradation mechanisms. The main idea is to photograph the cells repeatedly during an aging test under illumination that stays constant in an environment that does not change, and with photography settings that do not vary. The changes in the color of the cell components in the resulting pictures can be followed quantitatively, and using an experimental calibration the changes of color can be linked to the quantitative physical changes in the cell.

In practice the solar cells are photographed with a highly color-sensitive digital systems camera that is carefully white and color balanced. The illumination stays constant during the measurement of dozens of cells because the test cell stand is placed in a black box preventing the access of any stray light, and the white LED lamps are attached to the camera itself. Additionally the aging of the LEDs and the batteries that power the lamps is monitored. The test cell stand is colored neutral light gray to get better photographs of transparent solar cells. For transparent solar cells, the test cell stand should be made of a material that does not change color during the aging test (e.g., when exposed to UV light or water). The pictures are taken in RAW format and color balanced using a image processing software.

A quantitative method for extracting the amount of lost charge carriers using the camera imaging technique is presented in the literature [46] for DSCs with iodine electrolyte. The color of iodine electrolyte is strongly dependent on the concentration of iodine because it is strongly yellowish whereas the other electrolyte components are almost colorless. In RGB

color model, the yellow color is seen as the absence of blue value. Thus, the blue pixel value of the electrolyte color has been showed to correlate almost linearly with the concentration of iodine in the electrolyte over a wide concentration range of 0.025 - 0.1 M iodine [46]. The resolution of the method has been calculated to be $7.35 \cdot 10^{-4}$ M per blue pixel value [46]. The high resolution of the method is dependent on the correct exposure time in the pictures of the cells. The linear correlation between the blue pixel value and iodine concentration holds less accurately if the photographs are overexposed or underexposed, or if the background of the transparent electrolyte in the photographs is too dark.

The same principle of tracking the blue pixel value was in this thesis applied for PSC PEs for detecting the decomposition of dark-colored perovskite to yellow PbI_2. The technique was not calibrated to give an exact proportion of the decomposed perovskite because PSC PEs are not transparent, unlike the electrolyte. Due to this, the calibration could provide only the proportion of PbI_2 on the (front or back) surface of the cell instead of the whole active volume, as in the case of electrolyte in DSCs. The application of camera imaging on PSCs is discussed in detail in Section 4.4.

Image processing was in this thesis applied also for DSCs with cobalt complex electrolyte, which is discussed in more detail in Section 4.2.5. Cobalt complex electrolyte is close to colorless and transparent when it is fresh. Image processing showed, and is here reported in the literature for the first time, that while the electrolyte in the DSCs degraded, it turned more neutral gray in a linear fashion. Thus, when calibrated, a camera imaging system could be applied to the lifetime prediction of DSCs with cobalt complex electrolyte and likewise it is proven to work with iodine electrolyte.

3.2.4 X-ray powder diffraction

X-ray diffraction (XRD) is a method for the structural characterization of materials. In this work, it has been applied to investigating the presence of methylammonium lead iodide perovskite and its decomposition product, PbI_2, in PSCs. In XRD, monochromatic X-rays are projected on to a crystalline sample. The elastic scattering of the X-rays from the electrons in the atoms of the crystal structure [47] is measured.

XRD is explained by the theory of the diffraction of waves, the compressed basics of which are described next. The incident X-rays with wavevector k are assumed to be plane waves that scatter for one time

elastically and coherently from the crystalline material at point P, resulting in spherical waves with wavevector k′. With these assumptions, the wave scattered from the sample at point P and reaching the point of investigation outside the sample, B, is

$$A_{\mathrm{PB}} = A_0 e^{i\mathbf{k}\cdot(\mathbf{R}_{\mathrm{OP}}) - i\omega_0 t} \frac{e^{i\mathbf{k}'\cdot(\mathbf{R}_{\mathrm{PB}})}}{|\mathbf{R}_{\mathrm{PB}}|} \varrho, \tag{3.9}$$

where A_0 and ω_0 are the field strength and frequency of the incident waves, t is time, $\mathbf{R}_{\mathrm{OP}}$ is a vector from the source of incident waves (point O) to point P, $\mathbf{R}_{\mathrm{PB}}$ is a vector from point P to the point of investigation, B, and ϱ is a complex scattering density. The total scattered wave reaching point B, A_{B}, is given by integrating over the scattering region (the sample),

$$A_{\mathrm{B}}(t) \propto e^{-i\omega_0 t} \int\limits_{\text{sample}} \varrho(\mathbf{r}) e^{i(\mathbf{k}-\mathbf{k}')\cdot\mathbf{r}} d\mathbf{r}, \tag{3.10}$$

where r is the integration variable over the sample region [48]. Scattering density can be expressed in terms of a Fourier expansion of the reciprocal lattice vector **G** (assuming scattering from each lattice point), resulting in:

$$A_{\mathrm{B}}(t) \propto \sum_{\mathbf{G}} \varrho(\mathbf{G}) \int\limits_{sample} e^{i(\mathbf{G}+\mathbf{k}-\mathbf{k}')\cdot\mathbf{r}} d\mathbf{r}. \tag{3.11}$$

Integration in Eq. (3.11) results in term $\mathbf{G} + \mathbf{k} - \mathbf{k}'$ in the denominator. Thus, the integral may get significant contributions only when

$$\mathbf{G} = \mathbf{k}' - \mathbf{k}, \tag{3.12}$$

which is called the Laue condition [48]. Since the intensity of diffracted X-rays at point B is $|A_{\mathrm{B}}(t)|^2$, the contributions to intensity are also defined by the Laue condition.

The Laue condition is one of the corner stones of XRD. It implies that constructive interference happens only in directions fulfilling the Laue condition. Based on Eq. (3.11), an ideal infinite crystal would result in diffraction beams in δ function form. In practice, the nonidealities of the setup cause broadening and asymmetries of the beams that must be taken into account in the measurement design [49]. For instance, the width of the beam is inversely proportional to the crystal size [49]. The directions of constructive interference are in practice defined by spherical coordinate angles 2θ (angle between the incident and scattered X-ray) and ϕ (the rotation of the incident X-ray with respect to the sample). Additionally, the Laue condition expresses that the form of the resulting diffraction

pattern depends on the crystal structure of the sample via $\mathbf{G}$. XRD can thus be used for probing the properties of the crystal.

Bragg equation is an intuitive example about lattice properties that can be explored using XRD. From the properties of the reciprocal lattice vector

$$|\mathbf{G}_{hkl}| = G_{hkl} = \frac{2\pi}{d_{hkl}}, \tag{3.13}$$

where hkl are the Miller indices of a lattice plane and the separation between these lattice planes is d_{hkl}, and for the wavevectors due to elastic scattering

$$|\mathbf{k}' - \mathbf{k}| = 2\frac{2\pi}{\lambda}\sin\theta, \tag{3.14}$$

where λ is the wavelength of the X-rays, which gives the Bragg equation [48]:

$$\lambda = 2d_{hkl}\sin\theta. \tag{3.15}$$

The Bragg equation implies that X-rays are reflected from the (hkl) lattice planes of the crystal, and the shape and dimensions of the unit cell in the lattice can be determined based on the diffraction pattern [48]. The diffraction pattern can be used for various other applications, such as determining the crystal size or detecting crystal defects on the basis of extra or missing reflections in comparison to the assumption of an infinite perfect crystal [49]. Disordered systems, such as amorphous epoxy glue utilized in the encapsulation of PSCs, result in a broad bulge (or bulges) of diffraction instead of narrow diffraction peaks [49].

Even more information can be extracted from the data if the intensity of reflections is utilized: the contents of the unit cell can be analyzed [49]. The Fourier coefficients of ϱ in Eq. (3.11), called the structure factor, state the contribution of each unit cell to the intensity. Further, the structure factor arises from the contributions of each atom in the unit cell, called atomic scattering factor, that in turn arises from the contribution of single electrons [49].

For a single crystal, the structure analysis could be made by recording the Bragg reflections using a planar detector. The sample is gradually rotated with respect to the incident beam to collect data about the whole crystal structure. Inverse calculations are then applied for calculating the crystal structure [50].

PSCs are not single-crystalline samples but are in fact constructed from randomly oriented small crystals, hence powder diffraction is applied. In a powder, X-rays can hit any of the lattice planes, and in an ideal case,

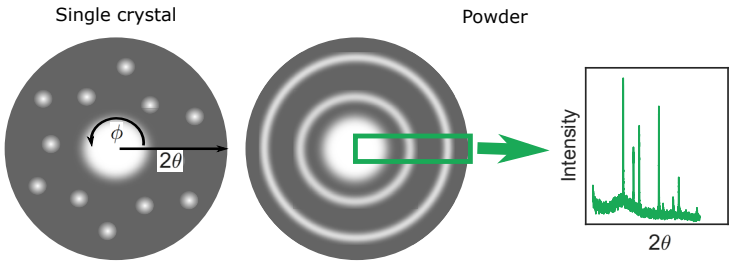

Figure 3.4. Schematics of the differences between the X-ray diffraction from a single crystalline and a powder (multicrystalline) sample. In X-ray powder diffraction, diffraction intensity is typically presented as a function of the angle between the incident and diffracted beams, 2θ.

rotation symmetry with respect to solid angle Ω leads to spherically symmetric diffraction pattern: diffraction forms conical trajectories with constant intensity instead of individual spots. If a planar detector is applied for investigating the diffraction from a perfect powder sample, nested circles are observed instead of the separate spots of a single-crystalline sample, which is illustrated in Fig. 3.4. Thus, only a stripe parallel to the radii of the circles need to be analyzed. It can be presented as a spectrum of intensity peaks as a function of θ.

Different compounds create XRD patterns that are typically distinguishable from each other. Thus, the presence of certain materials in a sample can be investigated by comparing the peak locations and intensities in the measured XRD curve to known materials. In this work, XRD is used for recognizing compounds present in the PSC samples by comparing them to the curves of the compounds of interest (i.e., perovskite and its decomposition product).

XRD curves should be compared with care, since there are several factors affecting the shape and intensity of the peaks, some of them being device-specific. For instance, the intensity of scattering is affected by the elements in the sample (intensity increases with atomic number Z), the unit cell (intensity increases if many lattice planes result in constructive interference in the investigated point), and θ (via absorption, temperature, and the geometrical setup of the measurement) [49]. The increased quantity of a compound will thus lead to a larger intensity of diffraction provided that other factors of scattering curve remain unchanged. Additionally, it should be noted that the depth of X-ray penetration is a function of the mass absorption coefficient of the material $c_{\text{absorption}}$ for which approximately [49]

$$c_{\text{absorption}} \propto \lambda^3 Z^3. \tag{3.16}$$

Thus, heavy elements such as Pb that the perovskite used in this study, $CH_3NH_3PbI_3$, contains, absorb X-rays efficiently. As a result, the surface of the PSC is more prominently present than the very interior of the cell in XRD curves in this work.

4. Main results and discussion

4.1 Role of impurities in the efficiency and stability of dye solar cells (Publication I and Publication II)

Impurities in DSCs have been mentioned in the literature [51, 52, 53, 54, 55, 56] to cause decreased efficiency and instability. In particular, dye and electrolyte could easily introduce impurities in the cell because they are not sintered unlike CE and the undyed PE. In this thesis, the effect of impurities of the electrolyte components and dye on the stability and efficiency of the cells was investigated in Publication I and II. It is clear that very large concentrations of impurities are likely to affect the performance of the cells. Here, we compared instead materials of highest purity available easily commercially to the materials further purified in a laboratory.

The investigated electrolyte consisted of iodine (I_2), 1-methyl-benzimidazole (NMBI), 1-propyl-3-methylimidazolium iodide (PMII), and guanidinium thiocyanate (GuSCN) dissolved in 3-methoxypropionitrile (MPN). For all electrolyte components but I_2 an effective laboratory-scale purification method was found (described in Publication I). Resublimated grade I_2 was considered to be as pure as practically possible and thus its purification was not investigated in this thesis. The investigated dye, N719 (cis-bis(isothiocyanato)-bis(2,20-bipyridyl-4,40-dicarboxylato)-ruthenium-(II)bis-tetra-butylammonium), was prepared and further purified according to a method described in Publication I, resulting in dye that produced less impurity peaks in nuclear magnetic resonance spectroscopy than the corresponding commercial dye. The impurity peaks were assigned to dye isomers of N719 that are not necessarily as efficient sensitizers as N719. Thus the prepared purified dye was expected to result in higher I_{sc} due to

the improved η_{LH}.

The effects of the purification of the dye, N719, on the efficiency and stability of the cells were investigated in Publication II. Two cell groups were prepared, either with the purified laboratory-made N719 or with commercial N719 used as received. There were five to seven DSCs in each cell group and all the cells contained electrolyte made of the purified above-listed materials. The IV curves measured after the cell assembly revealed no statistically significant differences in an independent samples t-test with 95% confidence level. Next, the cells were exposed to a 1,000-hour aging test at approximately 40°C under illumination (spectrum B in Fig. 3.1) connected to SCATU aging test system (see Section 3.1). The aged cell groups were compared with IV curve measurements, EIS performed at V_{oc} under 1Sun illumination, and camera imaging technique. None of these measurements resulted in a statistically significant difference between the cell groups (at 95% confidence level using the analysis of covariance with the incident illumination of each test cell during the aging test as a covariate).

Thus it was deduced that the dye isomers of N719 that were present as impurities in the tested commercial dye, did not significantly suppress the efficiency nor the stability of the DSCs. It seems that there is no need to purify the dyes beyond the purity level of commercial dyes. The result holds in the case that the standard deviations of the IV parameters of the cells are similar with respect to the IV parameter values than in this study. The situation might be different if the variations are clearly smaller and/or the cells are significantly more efficient than here. In this case, smaller differences between the DSCs with purified or unpurified dye result in statistical significance.

Next, the investigations were extended to the purification of each electrolyte compound. Seven groups of solar cells (with six samples in each group) were prepared in Publication I using the electrolytes presented in Table 4.1 and purified N719 in order to isolate the effect of impurities in each electrolyte component. The IV curves of the fresh cells were measured. Statistically significant differences were not found in η nor any other IV parameter in the analysis of variance test at 95% confidence level, i.e., the purification of any of the electrolyte materials was not detected to affect the performance of fresh DSCs.

Next, the cells were exposed to a 1,000h aging test at approximately 40°C under illumination (spectrum A in Fig. 3.1) connected to SCATU

Table 4.1. The electrolyte batches A-F tested in Publication I. All the electrolytes consisted of same materials (I_2, GuSCN, PMII, and NMBI dissolved in MPN) that were either purified (P) or used without further purification (U). I_2 was highly pure already as purchased so it was not purified separately.

Batch	I_2	GuSCN	PMII	NMBI	MPN
A	(P)	P	P	P	U
B	(P)	P	P	U	P
C	(P)	P	U	P	P
D	(P)	U	P	P	P
E	(P)	U	U	U	U
F	(P)	P	P	P	P

aging test system (see Section 3.1). The aging test revealed the drastic difference in the stability of the cell groups: groups A and E containing unpurified MPN as the solvent degraded much more quickly, which is illustrated in Fig. 4.1.

The unpurified electrolyte solvent did not result in any statistically significant differences in initial testing (including IV curves, EIS for the analysis of the series connected resistances of the cells, camera analysis for following the bleaching of the electrolyte, and spectral quantum efficiency measurements for investigating the operation of the PE) although it accelerated the degradation of the cells. This is an important observation from the viewpoint of quality control in cell manufacturing in laboratory and industrial environments: the adequate purity of the materials, in this case electrolyte solvent, cannot be ensured by measuring the performance of the fresh cells but it should be monitored by other means, e.g., directly from the solvent.

The quantity of electrolyte solvent in a DSC is clearly higher than the quantity of the other electrolyte components. Thus it seems reasonable that the impurities in the electrolyte solvent are the most significant factors for the lifetime of the cells when none of the unpurified materials is very impure but they are have all been purchased as pure as easily possible. The unpurified MPN contained reportedly water ($\leq$0.3%), chloride, and bromide ($\leq$50mg/kg) as impurities. Bubbles were detected to form in MPN when it was stirred with calcium hydride during the purification process applied in Publication I, after which the color of the liquid turned from slightly yellowish to completely transparent. The bubbles could have been hydrogen, which would suggest that the removed impurity was water.

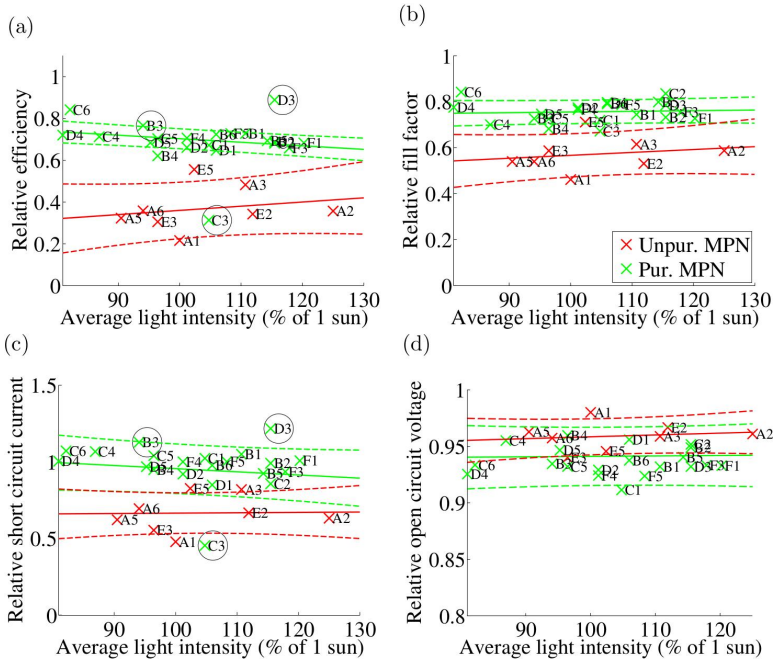

Figure 4.1. IV results normalized to the pre-aging values of each cell in cell groups A-F after 705h of aging shown as a function of the illumination intensity (measured separately for each cell). Groups A and E marked with bright red containing unpurified methoxypropionitrile solvent have degraded clearly more than the other groups marked with light green color. The regression lines and 70% confidence intervals drawn according to the method described in Publication I are also included. The cells marked with a black circle are excluded from the regression line calculation on the basis of Peirce's criterion. A reprint from Publication I under CC-BY license.

The aging test results were further analyzed to understand the aging mechanism activated by the impure solvent. Fig. 4.1 illustrates that after 705 hours of aging, all the cell groups suffered from the slightly decreased V_{oc} and clearly decreased FF that had decreased most in the cells with unpurified MPN. Additionally, I_{sc} of these cells had decreased whereas it had remained stable in the other cells. By the end of the 1,000-hour aging test, the degradation had proceeded so much that I_{sc} had decreased in all the cell groups, although the decrease was the most clear in the cells with unpurified MPN (the data shown in Publication I).

The operation of the PE of the cells was investigated by multiple measurement techniques. The EIS measurements performed in the dark at several different voltages revealed that the changes during the aging test in the R_{PE} and C_{PE} had been minor and additionally, the changes were similar in cells with both purified and unpurifed MPN. The minor changes in R_{PE} and C_{PE} suggest that PE operation has remained rather constant during the aging test. Liquid chromatography-mass spectroscopy (LC-MS) measurements were applied for investigating the chemical changes in the dye, and again, no differences between the cells with purified or impure MPN were not found. IPCE (incident photon to collected electron efficiency) measurements were applied for investigating changes in the charge transfer mechanisms η_{LH}, η_{INJ}, η_{COL}, and η_{REG} (see Section 2.1). IPCE performed at low light intensity in Publication I resulted in similar shaped spectra (apart from optical improvements related to electrolyte degradation, more information in Publication I) before and after the aging but the absolute values of the spectra had slightly decreased during the aging test. This suggests that η_{INJ} and/or η_{REG} had slightly changed but η_{COL} and η_{LH} had remained stable [27, 57]. The expected I_{sc} at 1Sun were calculated based on IPCE spectra to be 82-98% of the I_{sc} of the fresh cells, which proved that the changes in IPCE were indeed minor and did not account greatly for the performance degradation observed. Additionally, the I_{sc} expected based on low-intensity IPCE were higher than the I_{sc} in 1Sun IV measurements in all the cell groups. This suggests that the cells were suffering from the diffusion limitation in the electrolyte at 1Sun intensity, which was released at low intensity. In summary of the measurements related to PE, the PEs had not undergone severe degradation that would greatly affect the performance of the cells, and the degradation observed was similar in cells with purified and unpurified electrolyte. The degradation at PE does not explain the differing stability of these cells.

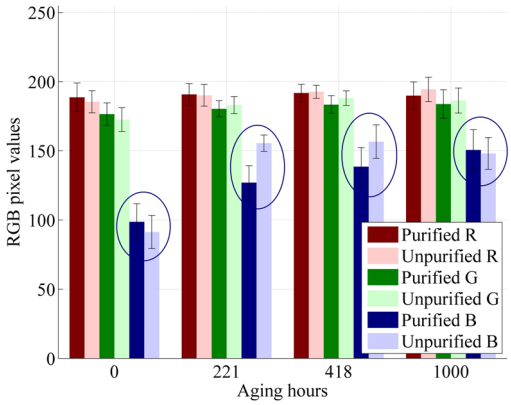

Figure 4.2. The RGB (red-green-blue) color values of the electrolyte in Publication I for cells with purified or unpurified electrolyte solvent, MPN. The fading of yellow color of the electrolyte is visible as an increase in blue values. The standard deviations of the values are also shown. The results are divided into two groups, cells containing purified electrolyte solvent and cells containing unpurified electrolyte solvent. A reprint from Publication I under CC-BY license.

The operation of CE and electrolyte were investigated by EIS performed under 1Sun illumination at V_{oc}. Both R_{CE} and R_{D} had increased during the aging in all the cells but the changes were larger in cells with unpurified MPN. The results imply at least electrolyte degradation and possibly also degradation at the CE. Image processing (see Section 3.2.3) results presented in Fig. 4.2 revealed that the purification of electrolyte solvent approximately halved the bleaching rate of the electrolyte during the aging test, i.e., the depletion of free iodine in the electrolyte. Thus the depletion of iodine seems to be the reason of the increased R_{D} that leads to the decreased FF of the cells. When the series connected resistances of the cell have increased drastically, they limit current even close to the short-circuit state of the cell, leading to the decreased I_{sc}.

As a conclusion, the purification of electrolyte solvent that was purchased at the highest purity commonly available from the suppliers, increased the lifetime of the cells by more than halving the main degradation mechanism of the cells, i.e., the bleaching of the electrolyte. The results suggest that the bleaching occurs due to chemical reactions activated by the impurities, possibly a very small concentration of water, in the electrolyte solvent. The purification of electrolyte solvent seems to be a straightforward way to clearly increase the lifetime of the cells. However, the purification of the N719 dye beyond the purity level of the commercial reference dye did not produce statistically significant improvements

in the efficiency nor the stability of the cells.

4.2 Preventing bleaching of electrolyte in dye solar cells (Publication I, Publication II, and Publication III)

The main degradation mechanism for all the DSCs in Publication I and II was identified to be electrolyte bleaching, i.e., the degradation of electrolyte through the loss of charge carriers (see Section 4.1). In the case of electrolytes with iodine redox couple, the loss of charge carriers leads to the fading of the yellowish color of electrolyte, in extreme cases resulting in completely transparent electrolyte, which is the origin of term "bleaching". There is an excess of charge carriers in typical fresh electrolyte. Thus, electrolyte bleaching does not immediately suppress the performance of cells but only after the concentration of the critical charge carrier has decreased so much that $I_{\mathrm{lim}} < I_{\mathrm{sc}}$ (see Section 2.1 for more information).

Electrolyte bleaching is a very commonly reported degradation mechanism in the literature under various stress conditions, such as UV light [46, 58, 17, 59, 60] or increased temperatures [54]. Several reactions have been suggested to lead to the bleaching of electrolytes with iodine redox couple, such as the formation of iodate that would be adsorbed on the TiO_2 surface, hydroxyl groups, OH radicals, or binding reactions between I_3^- and the TiO_2/dye ensemble [17, 54, 61, 62, 12]. However, effective methods for preventing or delaying the bleaching have been missing from the literature.

Thus, preventing the electrolyte bleaching was a major objective in this thesis. The special focus was in the prevention of bleaching under UV light. Importantly, the degradation is not stopped merely by using a UV light filter because they are always imperfect and managing the effect even with high quality filters is difficult as this work demonstrates. Three articles in this thesis, Publications PI, PII, and PIII, support each other on identifying methods for preventing electrolyte bleaching. Thus the results related to electrolyte bleaching are presented topic by topic instead of publication by publication in this Section. To ease the reading, the aged cell groups that are discussed in this Section are collected to Table 4.2. Apart from the differing parameters listed in Table 4.2, all the cells were aged in similar conditions (that are described in detail in each of the publications): for approximately 1,000h under approximately 1,000W/m^2

Table 4.2. The main parameters that are varied in the aging tests of cell groups A-H in Publications PI, PII, and PIII.

Cell group	Publication	Dye	Electrolyte solvent	Redox couple	UV filter
A	PI	N719	Unpur. MPN	0.05M I_2	No
B	PI	N719	Pur. MPN	0.05M I_2	No
C	PII	N719	Pur. MPN	0.10M I_2	No
D	PII	Z907	Pur. MPN	0.10M I_2	No
E	PIII	Z907	Pur. MPN	0.10M I_2	Yes
F	PIII	Z907	Pur. MPN	0.10M I_2	No
G	PIII	Z907	ACN	0.04M $[Co(bipy)_3](PF_6)_3$	Yes
H	PIII	Z907	ACN	0.04M $[Co(bipy)_3](PF_6)_3$	No

intensity UV and visible illumination at 40°C connected to the aging test system SCATU described in Section 3.1. The applied illumination spectrum was either spectrum A (no UV filter) or spectrum B (spectrum A + UV filter). It should be noted that although the UV filters applied in this thesis were of high quality, no UV filter can remove the UV illumination completely. Thus even the filtered irradiation contains traces of UV irradiation.

4.2.1 Increasing the concentration of charge carriers

A very straightforward method for delaying the performance degradation caused by electrolyte bleaching is to increase the concentration of charge carriers in the electrolyte. This would delay the start of current limitation caused by the loss of charge carriers.

The DSCs referred to as group B in Table 4.2 prepared in Publication I contained 0.05M I_2 and the cells lost more than 60% of their initial efficiency during the aging test. On the contrary, DSCs referred to as group F in Table 4.2 prepared in Publication III with otherwise the same electrolyte but with 0.1M I_2 sustained 70% of their initial efficiency during the aging test (data shown in Section 4.2.5).

This comparison suggests that the performance degradation could simply be compensated by adding extra charge carriers to the electrolyte. However, the concentration cannot be increased without a limit because

dark current (see Section 2.1) increases simultaneously, decreasing the efficiency of fresh cells. The increased concentration of charge carriers could lead to a stable performance in long-term (e.g., in a 1,000-hour aging test corresponding to one year operation under illumination) but does not prevent degradation in ultra-long-term because the actual degradation mechanism is likely not suppressed.

4.2.2 Initial investigations about filtering of ultra-violet light

Another straightforward way to suppress the degradation rate triggered by the exposure to UV light is UV filtering which is applied against UV-related degradation commonly in the literature [63, 8]. Initial investigations about the effectivity of UV filtering in preventing electrolyte bleaching triggered by UV light took place in Publication II.

Cells aged in Publication II referred to as group C in Table 4.2 were otherwise similar to group B prepared in Publication I but had a higher concentration of I_2, 0.1M. They were exposed to an aging test with a high-quality 390nm UV filter on top of the cells whereas no UV filter was applied in Publication I. As a result, the DSCs in Publication II with a UV filter passed the aging test without any statistically significant degradation whereas the DSCs in Publication I without a UV filter lost more than 60% of their initial efficiency during the aging test. However, camera imaging technique revealed that the UV filter decreased the bleaching rate of group C only to 0.020 ± 0.006mM/h from the 0.070 ± 0.015mM/h of group B [PI, PII]. Thus this initial comparison of two different aging tests suggested that UV filtering does not prevent the degradation via electrolyte bleaching but only slows it down. Therefore, UV filtering would not work as a sole solution for reducing the UV-related electrolyte degradation to the level that would enable decades of lifetime exposed to UV light. These investigations are continued in Section 4.2.5.

4.2.3 Electrolyte purification

The purification of electrolyte solvent was detected to suppress the electrolyte bleaching in Publication I, which was presented in detail in Section 4.1. All the cell groups tested in Publication I bleached to some extent during the aging test. However, the purification of electrolyte solvent, MPN, beyond the commercially easily available purity level drastically decreased the bleaching rate from 0.21 mM/h (group A in Table 4.2) to

0.07 mM/h (group B in Table 4.2) [PI, PII].

The bleaching likely originated from exposure to UV light because the cells were aged under spectrum A (Fig. 3.1) visible and UV illumination. According to the declaration of the manufacturer of the electrolyte solvent, a major impurity in the material was water that has been hypothesized to react with TiO_2 semiconductor under UV light [17, 58, 64]. This would explain the improvements in the stability of the cells achieved by material purification.

The bleaching observed in publication Publication I could in principle be triggered by, e.g., the inherently incompatible combination of cell materials. This option does not seem reasonable because the reference cells kept in the dark during the aging test maintained their initial efficiency. Thus, the bleaching is connected to the illumination. Visible light cannot at this stage be completely ruled out as a source of bleaching because we have not aged cells under pure visible light in this thesis. However, this hypothesis seems unlikely because quite similar cells have passed aging tests of multiple thousands of hours under pure visible light in the literature [65] and additionally, we have found no mentions about pure visible light triggering electrolyte bleaching in the literature.

4.2.4 Chemical tailoring with hydrophobic dye

Water absorbed into the cell could react with TiO_2 semiconductor under UV light [17, 58, 64], leading to electrolyte bleaching, which was also suspected in Publication I. Dye is adsorbed on the TiO_2 nanoparticles in DSCs, and thus a sufficiently hydrophobic dye could suppress the reaction rate. This hypothesis of chemical tailoring of the cell by hydrophobic dye was investigated in Publication II: would the change of dye from hydrophilic N719 to hydrophobic Z907 (cis-bis(isothiocyanato)-(2,2'-bipyridyl-4,4'-di- carboxylato)(2,2'-bipyridyl-4,4'-dinonyl)ruthenium(II)) dye suppress water-induced degradation?

In Publication II, two different aging tests were performed: one for cells with N719 dye (group C in Table 4.2) and another for cells with Z907 dye (group D in Table 4.2). The cells were otherwise similar and were aged under the same spectrum B (Fig. 3.1) illumination. The change of dye did not result in improved or statistically differing bleaching rate of the cells. The bleaching rate remained the same with Z907 dye (0.030 ± 0.006mM/h) than with N719 dye (0.020 ± 0.006mM/h) [PII]. Thus the use of hydrophobic dye does not seem to provide a solution for electrolyte bleaching.

4.2.5 Advanced investigations about the filtering of ultra-violet light and the change of redox couple

Publication I and Publication II demonstrated that the main degradation mechanism of iodine-based DSCs exposed to visible and UV illumination at least at a relatively low temperature of 40°C is the electrolyte bleaching. Both of these studies were made with the same type of iodine electrolyte. Two of the motivating questions of Publication III were if bleaching would be a significant degradation mechanism also in other types of electrolytes and if the effects of UV filtering would remain similar when the electrolyte is switched.

A cobalt complex electrolyte was selected as an alternative. In comparison with iodine redox couple, cobalt complex redox couples have more optimal redox potential that provides higher efficiency for the cells [66, 67] and they are less corrosive which could facilitate the application of flexible metal substrates in the cells [68, 69]. Additionally, cobalt electrolytes are almost colorless [PIII] which could be benefit from design viewpoint and in reverse cell configuration in which the light is coming into the cell from CE side. The stability of cobalt electrolytes has been investigated in the literature in few publications but one of the major disadvantages of cobalt electrolytes has often been poor stability [66, 68, 69, 70, 71, 72].

In total four groups of DSCs referred to as groups E-H in Table 4.2 were aged in Publication III. Groups E-F had iodine electrolyte and groups G-H had the alternative electrolyte, cobalt complex electrolyte. Groups E and G were placed under a high-quality UV filter with 400nm cut-off wavelength whereas groups F and H were aged without any UV filter. Otherwise the aging conditions were similar.

Measurements of cells with iodine electrolyte

Table 4.3 shows that the UV filter protected the iodine cells to such an extent that the post-aging efficiency of the cells was even higher than the initial efficiency of the cells. The increase is due to initial stabilization during the first tens of aging hours, which increased the current of the cells (data shown in Publication III). The efficiency of the unprotected iodine cells decreased by 30% from the initial values due to decreased FF and V_{oc}.

EIS results presented in Fig. 4.3 show a slight increase in R_{CE} for the iodine cells without a filter but otherwise the series connected resistances of the iodine cells remained stable or even decreased. Increase in R_{CE}

Table 4.3. Normalized IV curve parameters of the cell groups in Publication III after the 1,000h aging test. Derived from Publication III under CC-BY license.

Electrolyte	Iodine		Cobalt	
UV filter	No	Yes	No	Yes
Number of samples	6	3	4	6
$I_{sc,1,000h}/I_{sc,0h}$	1.1±0.3	1.4±0.4	0.2±0.1	1.4±0.3
$V_{oc,1,000h}/V_{oc,0h}$	0.92±0.03	0.96±0.03	0.91±0.04	1.03±0.04
$FF_{1,000h}/FF_{0h}$	0.7±0.2	0.9±0.3	0.16±0.03	0.6±0.2
$\eta_{1,000h}/\eta_{0h}$	0.7±0.2	1.2±0.3	0.04±0.02	0.9±0.3

indicates degradation either at CE or in electrolyte.

I_{sc} measured as a function of light intensity revealed a current limitation at higher intensities above 1Sun for the iodine cells aged without the UV filter (data shown in Publication III), which suggests a loss of charge carriers in electrolyte because current limitation was not visible in the fresh cells. Indeed, camera imaging results in Fig. 4.4 show electrolyte bleaching in both iodine cell groups although the UV filtering suppressed the bleaching rate by roughly 60% to a level that enabled stable performance till the end of the 1,000-hour aging test. IPCE results (shown in Publication III) support this conclusion because they indicate electrolyte bleaching (optical improvements at wavelengths in which iodine absorbs light and improved η_{COL} probably arising from reduced dark current) during the aging test.

LC-MS measurements were applied for investigating changes in the dye during the aging (the developed method is throughly described in our publication [73]). One degradation product of Z907 dye with m/z 907.3 was found from half of the iodine cells without the UV filter and from none of the cells aged under the UV filter. Thus it seems that the dye degraded to some extent under the UV exposure. Interestingly, this degradation product was found also from the cobalt cells with completely different electrolyte composition, which suggests that the formation of the compound is not related to the electrolyte components. The detected degradation of the dye is not the main reason for the performance degradation of iodine cells under UV exposure because a strong degradation of dye would have decreased the quantum efficiency of the cells. Here, the IPCE results (shown in Publication III) were actually improved rather than decreased during the aging.

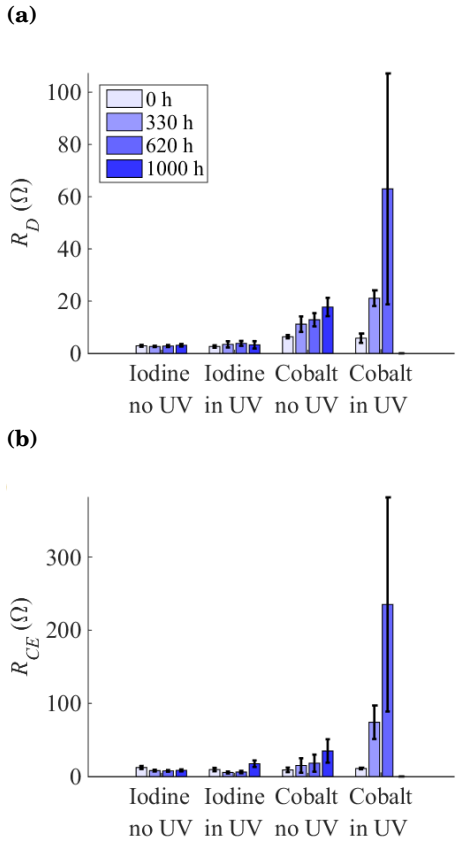

Figure 4.3. a) Diffusion resistance of electrolyte and b) charge transfer resistance at the interface between electrolyte and counter electrode resulting from electrochemical impedance spectroscopy performed at open circuit voltage under 1Sun illumination. Mean values and standard deviations are shown. Reprinted from Publication III under CC-BY license.

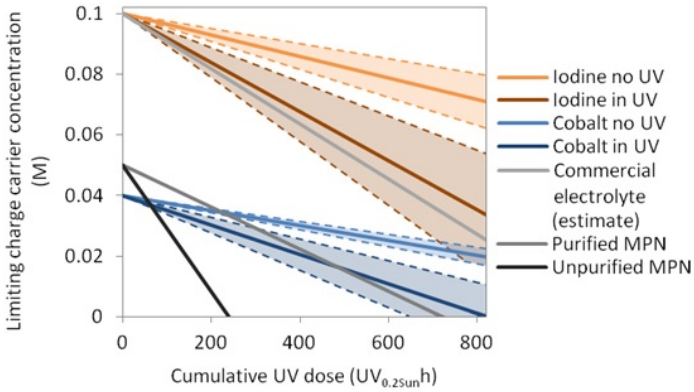

Figure 4.4. The estimated time development of the concentration of the limiting charge carrier in electrolyte during the aging test. The results are shown for iodine and cobalt electrolytes aged with and without UV filter in Publication III. For comparison, the results of Publication I are also shown ("Purified MPN" and "Unpurified MPN") as well as a literature result from [46] (details in Publication I). Reprinted from Publication III under CC-BY license.

Measurements of cells with cobalt electrolyte

Table 4.3 shows that the cobalt cells without the UV filter degraded practically completely by the end of the aging test through decreased I_{sc} and FF. The UV filter protected the cobalt cells enough for retaining 90% of the initial efficiency after the aging test (with I_{sc} increased because of initial stabilization at the beginning of illumination and decreased FF). This is among the best stability results for cobalt electrolytes in the literature — in fact, only one article applying UV light (although a UV filter was applied also there) in a 1,000-hour or longer aging test with approximately stable cells was found [70]. In most published tests with long duration and stable DSCs only visible light (LEDs) is applied [71, 74].

EIS results presented in Fig. 4.3 show massively increased R_D and R_{CE} for cobalt cells without the UV filter. Additionally, R_D and R_{CE} have increased clearly but not massively for cobalt cells aged under the UV filter. These changes indicate degradation in electrolyte and possibly also at CE.

I_{sc} measured as a function of light intensity revealed a current limitation at higher intensities above 1Sun for all cobalt cells (data shown in Publication III), which suggests a loss of charge carriers in electrolyte because current limitation was not visible in fresh cells. IPCE results (shown in Publication III) suggested the same: I_{sc} expected based on low-intensity IPCE measurements was clearly higher than the I_{sc} measured at 1Sun, which suggests electrolyte diffusion limitation under 1Sun illu-

mination that is released at low intensity, and improved η_{COL} probably arising from dark current that suppresses when the charge carrier concentration in the electrolyte decreases. Additionally, I_{sc} of the cobalt cells aged without the UV filter had dropped drastically even at low light intensities of 0.1-1Sun, suggesting dye degradation.

IPCE measurements performed at low light intensity and LC-MS measurements confirmed dye degradation in the cobalt cells aged without the UV filter (data shown in Publication III). The overall post-aging quantum efficiency of these cells was roughly 1/3 lower than the quantum efficiency of the cells aged under the UV filter. In LC-MS, ruthenium-based degradation products were found from both cobalt cell groups but the incidence of the compounds was higher for the cells without the UV filter. The IPCE of the cells with the UV filter had improved significantly during the aging test due to the initial stabilization of the performance (that also increased I_{sc} in Table 4.3) which demonstrates that dye degradation was not severe in the cells protected with the UV filter.

The method of camera imaging had not previously been applied for cobalt electrolytes. In Publication III, cobalt electrolyte was by camera imaging detected to turn from the original rather colorless form to darker neutral gray during the aging. This is a clear sign of chemical transformations in the electrolyte.

There is no published experimental calibration from the RGB pixel value of the electrolyte to the concentration of charge carriers for DSCs with cobalt electrolyte unlike for DSCs with iodine electrolyte [46]. However, the degradation rate of the cobalt electrolyte presented in Fig. 4.4 was in Publication III estimated pessimistically by correlating the post-aging color change of the cobalt electrolyte aged without the UV filter with the assumption of having no free charge left in the electrolyte (since these DSCs were practically fully degraded by the end of the aging test). The results revealed that the degradation rate of the cobalt electrolyte is halved but not completely prevented by the UV filter. Moreover, the degradation rate of the cobalt cells seems to be clearly lower than the rate of the iodine cells: for instance without the UV filter the limiting charge carrier concentration decreases 0.06M and 0.04M for iodine and cobalt cells, respectively, during the aging test.

Effects of ultra-violet light filtering and redox couple on electrolyte degradation

The experimental results of Publication III presented in Sections 4.2.5 and 4.2.5 show that whereas the iodine cells suffer moderately from UV exposure and the degradation is detected mainly in the electrolyte, the cobalt cells degrade massively under UV exposure via electrolyte degradation. Also the degradation of dye is stronger. The performance of the iodine cells did not decrease during the aging when the cells were protected by a UV filter but decreased by 30% without the UV filter. The performance of the cobalt cells suffered more during the aging test, resulting in 10% decrease with the UV filter (which still is among the best stability results for cobalt electrolytes in the literature, see Section 4.2.5) and practically full degradation without the filter. This is in accordance with the literature because the stability of cobalt electrolytes have been regarded lower than the stability of iodine electrolytes [72].

The degradation rates of the iodine and cobalt electrolytes were compared in Publication III. This investigation revealed for the first time in the literature that the cobalt electrolyte can actually be more stable under UV illumination (with or without a UV filter) than the traditional iodine electrolyte. The concentration of the limiting charge carriers in cobalt cells diminished at approximately 1/3 slower rate than in iodine cells both under UV filter or without it. It seems that the chemical tailoring of the cell composition by the change of redox couple can be an effective method for reducing the bleaching of electrolyte.

The reason for the faster performance degradation is actually the lower initial concentration of the redox couple instead of the inherently worse stability of it. The efforts on improving the stability of cobalt cells have to date been focused on improving the stability of the cobalt complex. However, Publication III shows that better blocking layers should be developed for cobalt cells. For instance, if the initial concentration of charge carriers could be increased to the level of iodine electrolyte, to 0.1M, without losing initial efficiency due to dark current, the cobalt cells could reach the stable performance of 3000 hours under a UV filter (neglecting other degradation mechanisms than electrolyte degradation).

In Publication III, the UV filtering reduces the bleaching rate of iodine and cobalt cells by approximately 60% and 50%, respectively. In other words, the UV filter did not stop the electrolyte degradation nor even reduced it in accordance with the UV light filtering efficiency of the UV

filter (which was 99% below 400nm for the filter applied in Publication III). There might be other factors present in addition to UV light triggering electrolyte bleaching, or the effects of UV light could correlate nonlinearly with the intensity of UV light. Nonetheless, UV filter alone is likely not an applicable solution for reaching long lifetimes for DSCs exposed to UV light but additional solutions are required. It seems that even the traces of UV light that pass the UV filter are extremely harmful in the long term, possibly because it triggers irreversible electrolyte degradation, which has been suggested in the literature [75]. The variation in the amount of emitted UV in different aging test devices might explain the discrepancy in some of the stability results in the literature, for instance for cobalt cells [PIII].

4.2.6 First steps of lifetime prediction of solar cells

Stability tests require a lot of manual work and absolute time even if they are accelerated ones, which is also discussed in Publication III and Publication VII. These practical reasons limit the possibility to extend the duration of tests even though the time scales targeted for example for building-integrated photovoltaics are on the range of decades. There is clearly a need of lifetime prediction although the literature on the topic remains scarce, the existing studies additionally focusing on other cell types than DSCs or PSCs [76, 77, 78].

The literature related to the stability of solar cells typically includes experimental aging testing and principal analyses on the stability of materials under different environmental conditions. The focus is typically on demonstrating certain lifetimes or linear extrapolation of the cell performance to the future.

However, for instance the results presented in Sections 4.1-4.2.5 demonstrate that phenomena are more complicated than that. Electrolyte bleaching that has in this thesis detected to be the main degradation mechanism in several DSC configurations with ruthenium-based dyes, proceeds in a rather linear way (see Fig. 4.2). Nevertheless, the degradation of electrolyte results in unlinearly evolving performance, which is illustrated in Fig. 4.5. The bleaching does not affect the performance of DSCs under 1Sun illumination at all until the concentration of the limiting charge carrier has decreased enough to limit the current generation of the cell at this intensity. Only after that, I_{sc} starts to decrease.

The understanding of degradation phenomena in solar cells could en-

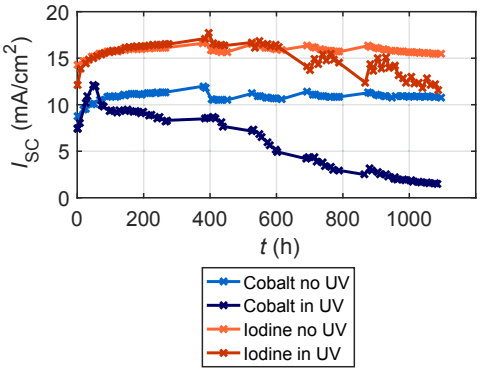

Figure 4.5. The evolution of short circuit current during the aging test under UV and visible illumination for four example dye solar cells either with iodine or cobalt electrolyte and with or without a UV filter. The short circuit current is decreasing mainly due to electrolyte degradation. The details of the aging test are presented in Publication III. Derived from Publication III under CC-BY license.

able more accurate estimations of lifetimes in future. The dominance of electrolyte bleaching in the degradation of DSCs investigated in Section 4.2 makes the bleaching a good example case for lifetime prediction.

The very first steps of lifetime prediction were taken in Publication I by comparing the detected starting time of the performance degradation to the moment estimated based on electrolyte bleaching rates. Based on the literature [79], the charge carrier concentration was estimated to start limiting I_{sc} at latest when the concentration decreases to 0.03M. This moment estimated based on camera imaging matched quite well with the actual start of performance degradation (e.g. with unpurified MPN, 100h and 120h, respectively).

The idea of lifetime prediction was further developed in Publication III. Image processing was utilized for the prediction of the lifetime of iodine and cobalt DSCs aged with or without a UV filter. The advantages of the lifetime prediction method in comparison to the traditional pass/fail-method without any prediction are demonstrated in Table 4.4. The traditional method can only determine if the DSCs were stable during the 1,000h aging test. The lifetime prediction based on the bleaching rate of the electrolyte gives estimates reaching to more than 2,000 hours (assuming that electrolyte bleaching is the only major degradation mechanism) with the same investment on the duration of the aging test and using such a fast, non-invasive measurement technique as camera imaging. Additionally, lifetime prediction enables the more systematic planning of the

Table 4.4. The comparison of the traditional method for the analysis of aging test results without any prediction, and lifetime prediction solely based on camera imaging (assuming that electrolyte bleaching is the only degradation mechanism). The latter method enables the estimation of future lifetimes whereas the first method does not. The example cell groups are DSCs from Publication III with either cobalt complex or iodine redox couple and aged either with or without a UV filter. Derived from Publication III under CC-BY license.

Cell group		Traditional method	Lifetime prediction	
Electrolyte	UV filter	Is the efficiency stable?	Period of stability (h)	Full degradation (h)
Iodine	Yes	Yes (120%)	2,200±400	2,800±400
Iodine	No	No (70%)	1,000±200	1,300±400
Cobalt	Yes	Yes (90%)	800±100	1,600±200
Cobalt	Yes	No (4%)	400±100	800±200

future targets of development. For instance, the data shown in Table 4.4 was in fact used in Publication III for concluding that the improvements in the blocking layer of cobalt DSCs would be valuable in increasing the cell lifetime, as discussed in Section 4.2.5.

These investigations are only initial ones but still demonstrate the future potential of lifetime prediction on the understanding of the stability of DSCs and PSCs. The full prediction of lifetime is challenging and still under research even for commercialized solar cell technologies [PVII]. However, it can be possible in the cases in which the degradation phenomenon in relation to the aging conditions is understood well enough.

4.3 Eased assembling and more even spacial performance distribution of dye solar cells by quasi-solidifying the electrolyte (Publication IV)

Many of the most promising DSC configurations involve liquid electrolyte that is sealed into the cell. Liquid electrolyte is a stability issue by its nature because it readily leaks or evaporates out from the cell if the sealing is compromised. This is unwanted firstly because the cell cannot operate without electrolyte and secondly because some electrolyte materials could form an environmental or health hazard if they would leak out from the cells in large scale applications. Foremost, liquid electrolyte is a manu-

facturing cost issue because the required careful sealing is challenging in large scale production. For instance, the roll-to-roll production and printing of solar cells are complicated when liquid electrolyte is involved.

Currently, liquid electrolyte is commonly injected or pumped into a sealed cell via small holes that are sealed afterwards (see Fig. 4.6a). The same procedure is utilized in both laboratory-scale and industrial production. The method has been detected to result in an uneven distribution of the electrolyte additives if the cells are large [19, 20, 18, 21]. The pumping distance between the holes (the order of centimeter) is very large in comparison with the thickness of the active volume of the cell (the order of micrometer). As a result, the flow of relatively bulky electrolyte additives is restrained and a higher concentration of them remains near the input hole than near the output hole, resulting in efficiency losses that could be even 35% [19]. The concentration gradient disappears slowly during time but complicates the initial assessment of the quality of the cell which again transforms into increased production costs in commercial production.

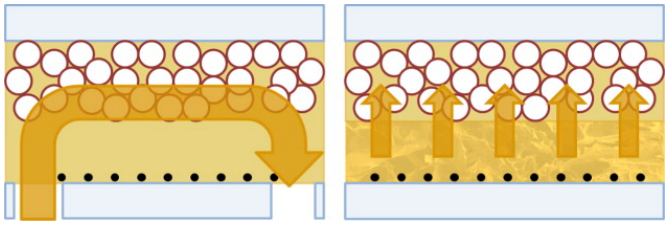

Figure 4.6. Electrolyte filling into a dye solar cell a) conventionally through filling holes b) using nanocellulose aerogel membrane developed in Publication IV. The arrows represent the direction of electrolyte flow. Reprinted from Publication IV with permission.

The challenges listed above can be tackled by developing solid or quasi-solid electrolytes that can be deposited with different methods. Quasi-solid electrolytes made by mixing additives (e.g., polymers or nanoparticles) to liquid electrolytes are attractive candidates because an already operational liquid electrolyte could be used as the basis of the quasi-solid electrolyte. The same solidifying method could also be compatible with multiple electrolyte recipes. However, the topic has been little investigated and for instance printable quasi-solid electrolyte recipes were not found at the time of Publication IV, which motivated the work (and also our other works not included in this thesis [80, 81, 82, 83]). Good quasi-solid electrolytes should be viscose enough to avoid flowing and leaking but simultaneously pass easily through the porous semiconduc-

Table 4.5. Mean IV parameters before the aging test for dye solar cells assembled with an aerogel layer or without it in Publication IV.

Aerogel	Number of cells	I_{sc} (mA/cm^2)	V_{oc} (V)	FF (%)	η (%)
Yes	3	11.7±1.4	0.70±0.01	57±3	4.7±0.8
No	4	9.7±0.7	0.75±0.01	66±2	4.8±0.2

tor nanoparticle layer to avoid performance loss.

In Publication IV, we propose a method for the quasi-solidification of liquid electrolyte by using a nanocellulose aerogel membrane acting as an infiltration matrix. The aerogel is made of never-dried bleached birch kraft pulp that is screen printed and freeze-dried on top of CE and reaches over 98% porosity (reported elsewhere [84]). The ultra high porosity allows very marginal effects on charge transfer. The liquid electrolyte is dropped on the membrane that gets wet like a sponge. The electrolyte is captured by the membrane so effectively that the cell can be sealed with electrolyte. After the cell assembly, the electrolyte spreads into the whole cell, which is illustrated in Fig. 4.6b. Thus, the cell can be assembled without external holes as opposed to the traditional method in Fig. 4.6a.

Table 4.5 shows that the aerogel method led to cells that were initially as efficient as the cells assembled in the traditional way. The aerogel layer appeared chemically inert based on EIS experiments performed in Publication IV: in addition to the initial efficiency, also diffusion in the electrolyte and charge transfer at the counter electrode remained similar to the conventional cells.

IV measurements of fresh cells shown in Table 4.5 demonstrated that I_{sc} was higher, V_{oc} lower, and FF lower with the aerogel than without it. Additionally, incident photon to collected electron (IPCE) measurements showed that the external quantum efficiency of the aerogelled DSCs was higher than without the aerogel (maximum IPCE approximately 60% and 50% with and without aerogel, respectively). A red shift in the data was also detected. These changes were in Publication IV associated with the differences in the electrolyte filling method schematized in Fig. 4.6, which results in a differing spatial distribution of voltage increasing agents that shift the conduction band of TiO_2 [19].

This hypothesis was tested. The IV results of DSCs with aerogel were compared to a single cell that we managed to assemble without external holes and electrolyte pumping and also without aerogel. This sample cell

produced similar IV result pattern to the aerogel cells. Thus, the changes in the IV results are probably linked to the differences in the electrolyte filling method instead of the aerogel layer itself. The aerogel membrane was deduced to lead to a more even distribution of the electrolyte additives than the conventional method that results in a more uneven distribution of localized initial efficiency in large cells.

Both cell types, with and without the aerogel, were equally stable in a 1,000-hour aging test at approximately 40°C under 1Sun illumination (spectrum A in Fig. 3.1) connected to SCATU (see Section 3.1), retaining approximately 90% of the initial efficiency during the aging test. Thus, the aerogel seems to remain inert also in long-term use which is a necessary prerequisite for a successful quasi-solidification procedure.

Conventional commercial iodide-tri-iodide electrolyte was used in Publication IV but this method could potentially be applied also to electrolytes containing other redox couples. This would be beneficial for industrial production because the production of DSCs in different colors requires the use of multiple different dyes which in turn typically requires a different electrolyte composition. The aerogel cells can, however, be chemically only equally stable to the liquid electrolyte inserted in the aerogel membrane. Therefore, very stable liquid electrolytes are required for filling the aerogel matrix when cells that remain stable in long-term are pursued.

4.4 Towards long-lived perovskite solar cells with highly reproducible performance (Publication V and Publication VI)

PSCs have inadequate stability for commercial applications and one main problem is perovskite decomposition caused by, for instance, exposure to humidity, visible or UV illumination, or the incompatibility of cell materials [16]. One of the promising candidate structures for more long-lived cells is the carbon based PSC without HTM, which is described in Section 2.2. Several successful PSC configurations with carbon have been reported [85, 41, 37, 86, 87], even with cell efficiency reaching 12.8% and remaining stable for more than 1,000 hours in ambient air under 1Sun illumination (with visible and UV light) [87].

Some of the carbon based cell configurations in the literature [41, 85, 86, 37] state to be printable and thus easily upscalable. This holds true for nanoporous TiO_2, silver paint, ZrO_2, and carbon. Additionally, TiO_2 compact layer can be deposited by spray pyrolysis that is a scalable process

[88]. However, a critical step, the infiltration of perovskite precursor, has remained manual. That is a manufacturing issue and can also result in increased variation in the performance of the assembled cells.

These facts created the motivation of Publication V for developing a truly easily upscalable, repeatable manufacturing method for long-lived PSCs in Publication V. The durability of the cells against normal indoor air humidity and UV-filtered visible and UV illumination was tested in Publication V. These results were so encouraging that the investigations were expanded to combined humidity and intense UV light stress in Publication VI, which the prepared cells withstood remarkably well. The aging tests gave also a possibility for successfully testing the camera imaging technique in the tracking of perovskite decomposition.

4.4.1 Development of cell manufacturing technique

The manufacturing technique for carbon based PSCs without HTM designed in Publication V is illustrated in Fig. 4.7. Steps a-g are traditional manufacturing methods applied before for PSCs. The final step of the inkjet printing of the perovskite precursor was developed in Publication V. Perovskite precursor has been printed directly on top of mesoporous TiO_2 or by printing individual perovskite precursor components separately in traditional PSC configurations [89, 90, 91]. However, these previously published methods were not adequate for carbon PSCs because after the inkjet printing of the perovskite precursor solution, ZrO_2 and carbon layers would have to be screen printed and fired at 400-500°C, destroying the perovskite.

Thus, the perovskite precursor was printed as the last manufacturing step. The effective infiltration of the precursor solution through many material layers (with total thickness of more than 10μm in Publication V) requires that the solution does not start to crystallize prematurely, which has been a limitation of the previously published inkjet infiltration methods. Additionally, the perovskite precursor ink should be compatible with the inkjet printer by not clogging the printer nozzles and in terms of the density, surface tension, and boiling point of the ink.

Keeping these requirements in mind, a suitable $CH_3NH_3PbI_3$ perovskite precursor ink was developed using lead iodide PbI_2, methyl ammonium iodide MAI, and 5-ammonium valeric acid iodide 5-AVAI dissolved in gamma-butyrolactone (a detailed description of the ink is presented in Publication V). 5-AVAI has been used as templating agent to improve the crystalline

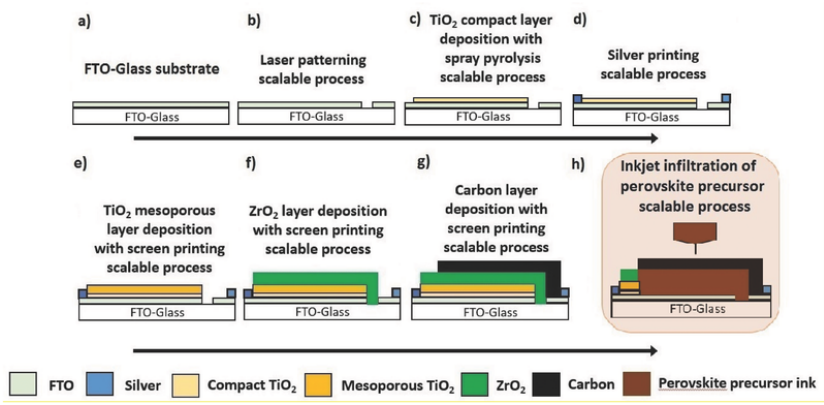

Figure 4.7. Scalable process for the production of HTM free carbon based perovskite solar cells. a) Fluorine doped tin oxide (FTO) coated glass substrate, b) laser patterning of the FTO layer, c) spray pyrolysis for compact titanium dioxide (TiO_2) layer deposition, and screen printing of d) silver contacts, e) mesoporous TiO_2 layer, f) insulating ZrO_2 layer, and g) porous carbon composite layer, and finally, h) inkjet printing of a controlled volume of perovskite precursor solution. Only scalable processes are highlighted here. The sintering steps consecutive to screen printing are not represented for better clarity. Reprinted from Publication V with permission.

network and charge-carrier lifetime of perovskite [41]. It was detected for the first time in Publication V that 5-AVAI also slows down the crystallization of perovskite precursor, facilitating spatially and volumetrically accurate printing of perovskite precursor. PSCs were prepared using the method illustrated in Fig.4.7 and optimized in respect of the volume of the printed perovskite precursor and the thickness of ZrO_2. The repeatability of the method was good, resulting for instance in $8.20\pm0.12\%$ (4 cells) efficiency with 2.9μm ZrO_2 thickness and 3.71μl perovskite precursor volume. The performance remained uniform during a three-week storage at room temperature in a vacuum container. The storage also resulted in increased efficiency: $9.42\pm0.14\%$. The improvements resulted from increased I_{sc}, FF, and V_{oc}, which were possibly caused by the further crystallization of the perovskite during the vacuum storage.

4.4.2 Perovskite solar cells durable against combined illumination and humidity

The stability of the cells prepared using technique described in Section 4.4.1 was investigated in Publication V. Nine PSCs without any additional sealing were exposed to a 1,046-hour aging test at normal laboratory room at open circuit under visible and UV illumination with a high-quality 400nm UV filter (spectrum B in Fig. 3.1) at $35°C$. The test at normal

indoor air humidity is rather harsh for PSCs because water causes perovskite decomposition leading to cell degradation [39, 40].

IV curve measurements repeated manually during the aging test in Publication V showed that the performance of the cells remained stable during the aging test: the mean efficiency is initially 6.4±0.6% and after the aging 6.7±0.3%. The only IV parameter that had experienced statistically significant changes in a t-test with 95% confidence level was FF that had decreased from 58±0% to 52±3%.

Image processing was applied before and after the aging test. The yellowing at the very edges of the active area of the PSCs was visible in the photographs but otherwise the cells seemed unchanged by the eye. The further analysis of the photographs shown in Fig. 4.8 revealed that the interior of the front and back sides of the PSCs had become lighter during the aging. The color change indicates changes in the cell materials in the interior of the cells even though the changes were so small that they were not visible using only the eye. The origin of the changes was investigated using XRD. A weak peak of PbI_2 that is a bright yellow decomposition product of $CH_3NH_3PbI_3$ perovskite (data shown in the Supplementary material of Publication V), was detected in the aged cells. Thus it seems probable that the lightening of the cells arises from the decomposition of perovskite that is so minor that it did not affect the performance of the cells in a 1,046-hour aging test (that corresponds to approximately one year of real-time operation under solar illumination). Even though the degradation is very minor at this stage, it could affect the performance of the cells in ultra-long timescale.

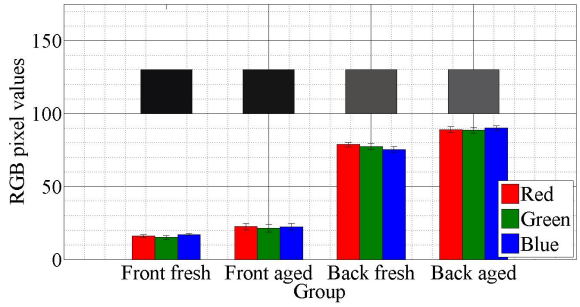

Figure 4.8. The mean RGB pixel values of the active area of perovskite solar cells before and after a 1,046-hour aging test. Higher values indicate lighter color. The color samples are also presented above each bar set. Reprinted from Publication V with permission.

However, the achieved stable performance of the PSCs without encapsu-

lation at indoor air humidity under illumination for 1,046 hours combined with highly reproducible initial performance and easily upscalable manufacturing process is a remarkable result. If the spray pyrolysis preparation of the compact TiO_2 layer can be replaced in future by a printing method, the manufacturing method will be not only scalable but also completely printable.

4.4.3 Perovskite solar cells durable against combined humidity and ultra-violet light illumination

PSCs prepared by the method described in Section 4.4.1 were further investigated in Publication VI by exposing them to normal indoor air humidity and intense UV light. UV light, especially combined with water as an impurity, is a major stress factor for DSCs, which is discussed in Publications I, II, and III. Water is one of the major stress factors of PSCs (Section 2.2) and concerns about UV light have been presented in relation to PSCs [63, 40]. Thus, combined UV light and air humidity is potentially a specifically severe stress for PSCs.

In Publication VI the PSCs were exposed to spectrum C illumination (Fig. 3.1) that corresponds to 1.5 times the total intensity of UV light in AM1.5G spectrum. A UV dose of 15kWh/m^2 that is required in the UV Preconditioning Test included in the IEC qualification tests of terrestrial thin-film solar cells [92] would thus be gained in roughly 300 hours, which depicts the harshness of the aging test. The cells were aged at open circuit conditions at approximately 40°C and 45% air humidity. Five PSCs were aged without any encapsulation and seven cells were aged with a thin epoxy glue encapsulation.

The efficiency of the PSCs without encapsulation increased at the beginning of the aging test from 7.1$\pm$0.5% to 7.7$\pm$0.5% but started to decrease by the IV measurement at 401h. The aging was ended after 751h of illumination when the mean efficiency had decreased by 26%, mainly due to a 29% decrease in I_{sc}. The cells with epoxy sealing endured a 1,002h aging test with stable efficiency. FF had decreased during the aging test by 13% but other statistically significant differences were not found.

Both cell groups were further investigated by other measurements. The results of camera imaging and XRD are shown in Figs. 4.9 and 4.10. Image processing results show a clear yellowing of the cells without encapsulation whereas the color of the encapsulated cells remains stable during the aging test. The source of color change was confirmed by XRD to be the

same than in Publication V: the aged sample without encapsulation has a clear PbI_2 peak as a result of perovskite decomposition whereas other samples present no signs of PbI_2. Additionally, the spectra of fresh and aged encapsulated cells are very similar, which indicates stability like the camera imaging result.

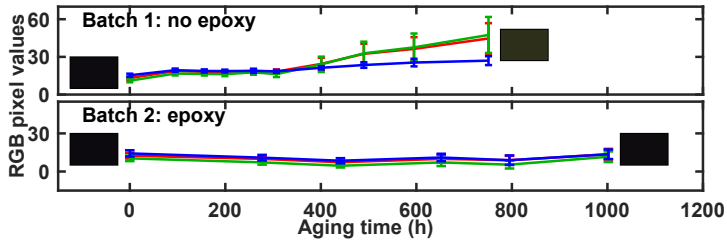

Figure 4.9. The evolution of the mean red, green, and blue RGB pixel values of the active area of perovskite solar cells with or without epoxy encapsulation pictured from the front side. Higher values indicate lighter color. The color samples from the first and last measurement are also presented. Reprinted from Publication VI under CC-BY license.

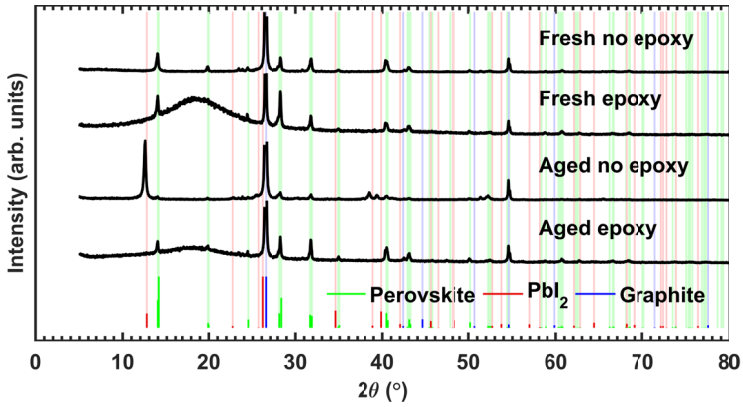

Figure 4.10. XRD results from the active area of the perovskite solar cells before and after the aging test. One sample cell from the group without encapsulation and from the group with epoxy encapsulation are shown. Additionally, the phase patterns of $CH_3NH_3PbI_3$ perovskite, lead iodide, and graphite are presented. The largest 26.4° peak is cut in this graph. Reprinted from Publication III under CC-BY license.

Publication VI demonstrates the exceptional stability of the HTM-free carbon based PSCs prepared by fully scalable techniques presented in Publication V. The PSCs without any additional encapsulation maintain stable performance under heavy 1.5Sun UV illumination and approximately 45% air humidity for at least 250 hours. Furthermore, the cells encapsulated simply by a thin layer of epoxy glue endure a similar 1,002-hour aging test without any detectable changes in the active area of the

cells. These results give a strong evidence that PSCs as a technology are not inherently unstable but future developments could lead to a market breakthrough.

Publication V and VI also jointly demonstrate that camera imaging technique can be applied as a non-intruding in-situ tool for detecting the early stages of the degradation of PSCs. In particular, the decomposition of $CH_3NH_3PbI_3$ perovskite to lead iodide yellow in color is readily detected.

4.5 Improving methodological quality of stability research of perovskite and dye solar cells (Publication VII)

Better reporting and more uniform stability testing methods have been called for by several researchers and publishers in the field of PSC and DSC stability during recent years [12, 93, 63, 94, 38, 95]. Although the number of articles published related to PSCs and DSCs is increasing (in the case of PSCs, even exploding [96]), the state of stability research remains unsatisfactory. This might originate from the belief that the issues are not wide-spread or the lack of knowledge on how to improve the situation.

Publication VII maps quantitatively the methodological quality of the very recent aging tests of PSCs and DSCs to determine the extent of the deficiencies in practices and to give practical suggestions on improving them. Publication VII is the first literature analysis in the field that focuses on the methods of stability testing instead of the results of the stability tests. The vast source material of 157 articles concerning PSCs and DSCs consisted of all the journal articles using stability-related terms in their titles, published during 2016 (for PSCs) or 2015-2016 (for DSCs), and listed in Web of Science (a detailed description of search terms in Publication VII). In total 262 aging tests were analyzed.

The first finding of the analysis in Publication VII was the extremely small number of aged cells that were reported in the published articles. In only 35% of the aging tests the results are shown (or the aging tests is reported to have been performed) for more than one cell in a cell group and the number of cells is actually reported. Fig. 4.11 illustrates that presenting the results of aging tests only for one cell in each cell group is the overwhelmingly most typical case. Deductions that are based on single cells are clearly not statistically reliable. Some aging tests could have been performed for more cells but only the results of a sample cell are pre-

sented in the published article. However, there is no way for the scientific audience to tell which one is the case unless the number of aged cells is reported. Additionally, it is common to omit the reporting of the group size even though there would have been multiple cells. Not reporting the group size greatly decreases the impact of the resulting article because the audience cannot estimate the reliability of the results. Testing only single cells or very small groups of cells can easily generate false positive or negative results. Thus, statistically acceptable group sizes should be targeted. Fig. 4.11 illustrates that groups of ten cells or more have been aged in approximately only 10% of the aging tests. Nevertheless the existence of this kind of tests demonstrates that achieving group sizes that are on a statistically acceptable level is possible.

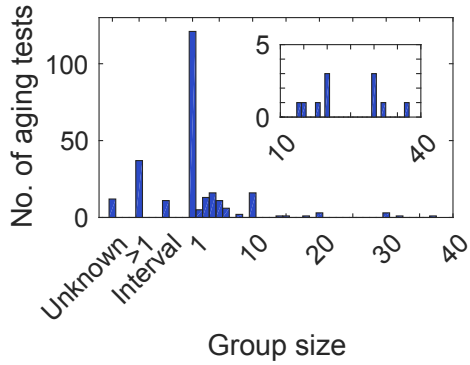

Figure 4.11. The distribution of the number of samples in each cell group (Group size) in the investigated aging tests of perovskite and dye solar cells. The number of tests with unknown group size, tests in which the group size is not mentioned but the samples are referred to in plural form (>1), and tests in which an interval (e.g., 3-6 cells) is reported, are also listed. Reprinted from Publication VII.

The optimal group size depends on three factors: desired reliability (e.g., the applied confidence level of a statistical test used for result analysis), expected effect (e.g., the expected difference in the post-aging efficiencies of the cell groups), and expected variations (e.g., the standard deviations inside the cell groups) [PVII]. The higher reliability of the aging test is desired or the more variations there are in the resulting data, the more cells are required in the aging test. On the other hand, the larger the expected effect is, the less cells are needed. In Publication VII, a method for estimating the optimal group size for an aging test of two cell groups based on the calculation of the statistical power of t-test is presented as an example of the analytical determination of required group size.

The second major deficiency found from the aging tests of PSCs and

DSCs in Publication VII was the insufficient reporting of the test conditions. It complicates the interpretation and the comparison of aging tests in the literature. Imperfect reporting could also generate results to the literature that are seemingly contradictory but originate from differing test conditions.

Fig. 4.12 illustrates that the intensity or even the presence of UV light remains unknown in most illuminated aging tests. UV light is a severe stress factor in many PSC and DSC configurations, which has been discussed in Sections 4.2 and 4.4.3, and could greatly affect the lifetime of the cells in the aging test. Based on the investigated articles, it seems that a commercial solar simulator with a calibration cell is commonly regarded to be a sufficient description of the aging illumination spectrum. However, in the context of UV-induced degradation, this is not enough because many standards for the accuracy of solar simulators do not specify the spectrum below 400 nm wavelength at all (e.g., SFS-EN 60904-9, JIS C 8912, and ASTM E927 for AM1.5G [PVII]). A simulator could be very accurate in the visible region but inaccurate at UV region, in an extreme case even emit no UV light at all. Thus, the comparison of illuminated aging tests would be greatly eased if the spectrum of the applied illumination would be presented in the articles.

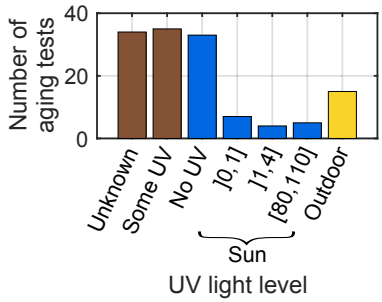

Figure 4.12. The applied ultra-violet light in all but dark aging tests investigated in Publication VII. In "Unknown" cases it could not be determined based on the published article if ultra-violet light had been applied or not and in "Some UV" cases the presence of ultra-violet light was reported in the article but the intensity was not. "No UV" cases are illuminated aging tests with only visible light. Quantitatively reported values are presented in Suns (0-1, 1-4, or 80-110 times the intensity the UV part of AM1.5G spectrum). Also outdoor tests are presented. Reprinted from Publication VII.

Another example of the insufficient reporting of test conditions is the temperature and humidity in aging tests. It was detected in Publication VII that the majority of all the investigated aging tests omit the reporting of one or both of the parameters, or report them only qualitatively

(typically "ambient"). The actual values of temperature but in particular humidity could vary greatly in these tests. The daily and seasonal variations of indoor air humidity are in Publication VII demonstrated to be so large that the actual value could be almost anything between close to zero and 100% (data not shown here), and in illuminated tests the cells could experience temperatures of dozens of degrees above the ambient temperature depending on the proportion of infra-red irradiation. The variations in humidity definitely affect the lifetime of cells that are sensitive to moisture (e.g., most PSC configurations) and aged without encapsulation. The increased temperature could also generate unwanted reactions such as phase-transition in perovskite or the decomposition of cell materials.

The effectivity of the stability research of PSCs and DSCs could be greatly increased if the environmental conditions (at least the main factors i.e. humidity, temperature, the type of illumination, and the electrical state of the cells) during the aging test were reported more carefully. Better reporting necessarily requires more careful tracking of the environmental parameters by measurements.

Fig. 4.13 illustrates how test durations and post-aging efficiencies are distributed in the aging tests investigated in Publication VII. Typically, the tests are ended with post-aging efficiency of 80-100% of the original efficiency. Although the published tests are typically ended with efficiencies that can be regarded as being stable, the test durations vary. The aging tests of DSCs peak at 1,000h, possibly because this test duration has established as a default test duration during the decades. The aging tests of PSCs are strongly peaked to shorter than 250h tests and the phenomenon is the clearest for the illuminated tests. PSCs are a new technology. Possibly because of that, short test durations are currently still common and seem to be regarded to be sufficient for publication. The very strong peaking of illuminated aging tests at short test durations also suggests that illumination is still a severe stress factor for PSCs.

The length of the aging test and the post-aging efficiency of the cells are variables with a strong reverse correlation. However, the combination is merely a question of test design because one can select the length of the test so that it results in the desired post-aging efficiency. The progress in the stability research of PSCs and DSCs would benefit from more aging tests extended to show the signs of degradation in the tested cells. This would give basis for the analysis of aging mechanisms instead of merely demonstrating certain lifetimes. The shortcomings in the methods of

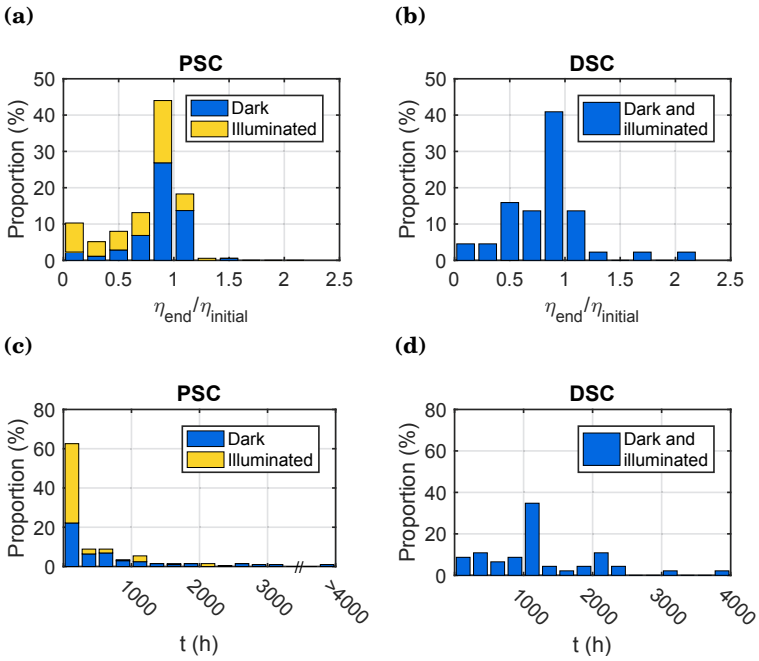

Figure 4.13. The distributions of final efficiency in proportion to the initial efficiency in the aging tests of a) perovskite b) dye solar cells, and the duration of the aging tests of c) perovskite d) dye solar cells. The illuminated and dark tests are shown separately for perovskite solar cells. In the case of dye solar cells, they are combined together. All the final efficiencies are the efficiencies of the most stable cell group in the aging test. Reprinted from Publication VII.

aging tests detected in Publication VII can hamper the progress of the stability research of PSCs and DSCs. Improvements are needed urgently. The organization of international summits for determining standards for the aging tests of PSCs and DSCs is suggested in Publication VII for engaging the scientific community in the process.

5. Summary and conclusions

This thesis focuses on the degradation phenomena and increasing the lifetime of DSCs and PSCs. These are critical factors in bringing the technologies towards commercialization in order to provide more affordable and more widely applicable photovoltaics.

The work commenced by investigating how the performance and stability of DSCs are affected by impurities in the dye or electrolyte. The effects of minor concentrations of impurities found in commercially available dyes and electrolyte components that are already of rather high purity were investigated in Publication I and Publication II. Contrary to the prior beliefs and initial hypothesis, the purification of dye (N719) was detected to affect neither the performance nor the stability of DSCs in Publication II. The same held for the investigated additives of iodine electrolyte (GuSCN, PMII, NMBI). No differences with regards to performance, series connected resistances or the kinetic charge transfer mechanisms were found from the fresh cells with purified or the unpurified electrolyte solvent, MPN, either. However, the purification of the solvent resulted in more than a halved rate of electrolyte bleaching (loss of charge carriers in electrolyte) and an increased lifetime during a 1,000-hour aging test under visible and UV light. Bleaching was the main degradation mechanism for the DSCs in the aging test. The main impurity in MPN removed by the purification was most likely water, which was suspected to trigger electrolyte bleaching under exposure to UV light. Thus, it was shown in Publication I that the impurities could greatly affect the lifetime of the cells even though no differences in the operation of the cells were initially found.

The second major topic in this thesis was the prevention and suppression of electrolyte bleaching in DSCs, which was investigated in Publications I-III. Electrolyte bleaching was detected to be the main degrada-

tion mechanism in DSCs with iodine or cobalt complex redox couple and ruthenium-based N719 or Z907 dyes at low temperatures (approximately 40°C) under visible and UV light. The increase of the initial concentration of the limiting charge carrier in the electrolyte led to increased period of stability in the aging test because it took longer before the charge carriers had diminished enough to start limiting the current of the cell. Nevertheless, the increase of charge carrier concentration did not affect the bleaching rate. Chemical tailoring of the cell composition by changing the dye from hydrophilic N719 to hydrophobic Z907 did not affect the bleaching rate either. Several methods were found to suppress the bleaching rate in addition to the above-mentioned purification of electrolyte solvent: the application of UV filter decreased the bleaching rate by 50-60% and the change of redox couple from iodine to a cobalt complex by approximately 30%. However, no methods for completely preventing the bleaching were found.

It was very unexpected that the UV filtering reduced the bleaching this little because the UV filter had a 99% filtering efficiency. Either there are other mechanisms triggering bleaching in addition to UV light, or the effects of UV light on bleaching are nonlinear. Nevertheless, UV filtering alone does not seem to be the solution for DSCs so that they would remain stable for decades under UV exposure, which contrasts with typical suggestions in the literature. Clearly, additional methods must be applied.

The bleaching rate of the cobalt complex electrolyte was actually lower than the bleaching rate of the iodine electrolyte, which is interesting. In this work, the performance degradation proceeded more quickly in the cobalt cells than in the iodine cells because of the lower initial concentration of the limiting charge carrier in the cobalt electrolyte. However, cobalt cells could be more long-lived than iodine cells if better blocking layers would be developed for cobalt cells and, as a result, the concentration of charge carriers in cobalt electrolytes could be increased without losses to the initial performance.

The work in this thesis demonstrates the persistence of bleaching as the main degradation mechanism of DSCs. However, the dominance of bleaching also means that tackling it could lead to long-lived DSCs, at least under those conditions applied in this thesis and thus, further investigations on the topic should be continued. Firstly, the effects of UV light should be separated from the possible effects of pure visible light by testing cells under pure visible light. Since even minor concentrations of

water seem to accelerate the bleaching under UV and visible light, one path to proceed towards more stable DSCs would be the application of more efficient sealing (such as glass-frit sealing) to cobalt electrolyte with dried solvent and increased charge carrier concentration. The switching of TiO_2 to another semiconductor or the modification of TiO_2 layer could be beneficial, which also has been investigated in the literature [63].

Bleaching was detected to proceed in a rather linear way from the commencement of the stress but the performance degradation started only after the diminished concentration of the limiting charge carrier began to limit the current of the cell. This prevents the extrapolation of cell lifetimes based on sole IV measurements. However, the lifetime of the cells with regards to bleaching could be estimated beyond the duration of the aging test by determining the bleaching rate of the cells (for instance by using the fast and non-destructive camera imaging technique, as utilised in this study). The first steps of this kind of lifetime prediction analysis were demonstrated in this thesis and the method could be applied also to other aging mechanisms and stress factors. Lifetime prediction should be explored further in the future because it could bring new insights to stability research and also save aging test hours.

The third part of this thesis work is the development of a method for quasi-solidifying liquid electrolytes in Publication IV. A recognized issue in DSCs is the liquid electrolyte that complicates the sealing process of the cell and can leak or evaporate from the cell, causing cell failure and potential environmental hazards if the electrolyte volume is large. Nevertheless, many of the most promising DSC configurations involve liquid electrolyte.

In Publication IV, a nanocellulose aerogel membrane was fabricated by screen-printing and freeze-drying, and applied as an infiltration matrix for liquid electrolyte with an iodine redox couple. The membrane captured the electrolyte so effectively that DSCs could be sealed after introducing the electrolyte into the cell. The method resulted in a spatially more even initial distribution of electrolyte additives than the traditional fabrication method of pumping the electrolyte through the cell. Otherwise the cells with and without the aerogel were similar with regards to initial performance and properties, and also stability based on a 1,000-hour aging test under UV and visible illumination. Thus, the aerogel membrane seems to be inert in the cell and applicable for the quasi-solidification of the electrolyte. The method could also be suitable for other types of electrolytes

than applied here, which could be investigated in the future.

The fourth topic investigated in Publication V and Publication VI was the development of PSCs that are long-lived, have a reproducible performance, and can be manufactured by upscalable processes. PSCs are generally regarded as unstable but promising results have been obtained with carbon based PSCs without HTM. A technique was developed for inkjet printing the perovskite precursor solution through all the layers of carbon based PSCs without premature crystallization of the solution. The repeatability of the technique was good (e.g., $8.20\pm0.12\%$ efficiency for a set of four cells).

The performance of the cells was tested and found to increase during a 3-week storage period in a dark at room temperature inside a vacuum container. The stability tests were continued by exposing another set of cells to a 1,000h aging test under visible and UV illumination with a UV filter in air at $35^{\circ}\mathrm{C}$. The cells endured the combined humidity and illumination stress without performance degradation even though they did not have any encapsulation. The tests were continued by exposing similar cells to 1.5Sun UV illumination at $40^{\circ}\mathrm{C}$ temperature and 45% air humidity. The PSCs remained stable for more than 250h but the performance started to decrease slowly after that. However, the PSCs with a simple encapsulation using a thin layer of epoxy glue remained stable for 1,000 hours.

These results, that are among the best stability results achieved for PSCs, give strong evidence that PSCs are not inherently unstable as a technology. Additionally, these results show that PSCs can be durable against UV light even though they would contain TiO_2. Using an optimized configuration, a good durability against both moisture and UV light can clearly be achieved.

This thesis was concluded by analyzing the methodological quality of the recently published aging tests of PSCs and DSCs in Publication VII. These aging tests were found to have been reported for far too few cells in each cell group, and they also suffered from too superficial reporting of aging test conditions. These deficiencies are wide-spread and could generate false conclusions regarding the lifetime, and complicate the comparison of studies in the literature. The situation would be improved by better test design and a more detailed reporting of the tests. Additionally, the published aging tests have commonly been designed to result in stable post-aging efficiencies although the test durations vary and, especially in the

case of PSCs, are short. Lengthening the aging test durations beyond the stable time period of the test solar cells would provide more information about the degradation mechanisms of the cells. To incorporate these improvements, more standardized testing procedures need to be established and adopted.

References

[1] Fermentas Inc. The Paris agreement, October 2017. URL http://unfccc.int/paris_agreement/items/9485.php.

[2] General Assembly UN. Transforming our world: The 2030 agenda for sustainable development. Technical report, UN, General Assembly, 2015. URL https://sustainabledevelopment.un.org/content/documents/21252030%20Agenda%20for%20Sustainable%20Development%20web.pdf.

[3] International Energy Agency IEA. Renewables information: Overview (2017 edition). Technical report, IEA, International Energy Agency, 2017. URL https://www.iea.org/publications/freepublications/publication/RenewablesInformation2017Overview.pdf.

[4] International Renewable Energy Agency IRENA. Renewable capacity statistics 2017. Technical report, 2017. URL http://www.irena.org/DocumentDownloads/Publications/IRENA_RE_Capacity_Statistics_2017.pdf.

[5] Seth B. Darling and Fengqi You. The case for organic photovoltaics. *RSC Adv.*, 3:17633–17648, 2013. doi: 10.1039/C3RA42989J. URL http://dx.doi.org/10.1039/C3RA42989J.

[6] SolarPower Europe. Global market outlook 2017-2021. Technical report, SolarPower Europe, 2017. URL http://www.solarpowereurope.org/reports/global-market-outlook-2017/.

[7] International Energy Agency IEA. 2016 snapshot of global photovoltaic markets. Technical report, IEA, International Energy Agency, 2016. URL http://www.iea-pvps.org/fileadmin/dam/public/report/statistics/IEA-PVPS_-_A_Snapshot_of_Global_PV_-_1992-2016__1_.pdf.

[8] Muhammad Imran Asghar, Kati Miettunen, Janne Halme, Paula Vahermaa, Minna Toivola, Kerttu Aitola, and Peter Lund. Review of stability for advanced dye solar cells. *Energy Environ. Sci.*, 3:418–426, 2010. doi: 10.1039/B922801B. URL http://dx.doi.org/10.1039/B922801B.

[9] Syed Ghufran Hashmi, Merve Özkan, Janne Halme, Shaik Mohammed Zakeeruddin, Jouni Paltakari, Michael Grätzel, and Peter D. Lund. Dye-sensitized solar cells with inkjet-printed dyes. *Energy Environ. Sci.*, 9:2453–2462, 2016. doi: 10.1039/C6EE00826G. URL http://dx.doi.org/10.1039/C6EE00826G.

[10] Wei Zhang, Miguel Anaya, Gabriel Lozano, Mauricio E Calvo, Michael B Johnston, Hernan Míguez, and Henry J Snaith. Highly efficient perovskite solar cells with tunable structural color. *Nano letters*, 15(3):1698, 2015. doi: 10.1021/nl504349z. URL http://dx.doi.org/10.1021/nl504349z.

[11] Giles E. Eperon, Victor M. Burlakov, Alain Goriely, and Henry J. Snaith. Neutral color semitransparent microstructured perovskite solar cells. *ACS Nano*, 8(1):591–598, 2014. doi: 10.1021/nn4052309. URL http://dx.doi.org/10.1021/nn4052309. PMID: 24467381.

[12] Andreas Hinsch, Welmoed Veurman, Henning Brandt, Katrine Flarup Jensen, and Simone Mastroianni. Status of dye solar cell technology as a guideline for further research. *ChemPhysChem*, 15 (6):1076–1087, 2014. ISSN 1439-7641. doi: 10.1002/cphc.201301083. URL http://dx.doi.org/10.1002/cphc.201301083.

[13] Andrea Reale, Lucio Ciná, Ambra Malatesta, Riccardo De Marco, Thomas M. Brown, and Aldo Di Carlo. Estimation of energy production of dye-sensitized solar cell modules for building-integrated photovoltaic applications. *Energy Technology*, 2(6):531–541, 2014. ISSN 2194-4296. doi: 10.1002/ente.201402005. URL http://dx.doi.org/10.1002/ente.201402005.

[14] Woon Seok Yang, Jun Hong Noh, Nam Joong Jeon, Young Chan Kim, Seungchan Ryu, Jangwon Seo, and Sang Il Seok. High-performance photovoltaic perovskite layers fabricated through intramolecular exchange. *Science*, 348(6240):1234–1237, 2015. ISSN 0036-8075. doi: 10.1126/science.aaa9272. URL http://science.sciencemag.org/content/348/6240/1234.

[15] Martin A. Green, Yoshihiro Hishikawa, Wilhelm Warta, Ewan D. Dunlop, Dean H. Levi, Jochen Hohl-Ebinger, and Anita W.H. Ho-Baillie. Solar cell efficiency tables (version 50). *Progress in Photovoltaics: Research and Applications*, 25(7):668–676, 2017. ISSN 1099-159X. doi: 10.1002/pip.2909. URL http://dx.doi.org/10.1002/pip.2909. PIP-17-089.

[16] M.I. Asghar, J. Zhang, H. Wang, and P.D. Lund. Device stability of perovskite solar cells - a review. *Renewable and Sustainable Energy Reviews*, 77(Supplement C):131 – 146, 2017. ISSN 1364-0321. doi: https://doi.org/10.1016/j.rser.2017.04.003. URL http://www.sciencedirect.com/science/article/pii/S1364032117304756.

[17] Simone Mastroianni, Imran Asghar, Kati Miettunen, Janne Halme, Alessandro Lanuti, Thomas M. Brown, and Peter Lund. Effect of electrolyte bleaching on the stability and performance of dye solar cells. *Phys. Chem. Chem. Phys.*, 16:6092–6100, 2014. doi: 10.1039/C3CP55342F. URL http://dx.doi.org/10.1039/C3CP55342F.

[18] Kati Miettunen, Janne Halme, and Peter Lund. Spatial distribution and decrease of dye solar cell performance induced by electrolyte filling. *Electrochemistry Communications*, 11(1):25 – 27, 2009. ISSN 1388-2481. doi: https://doi.org/10.1016/j.elecom.2008.10.013. URL http://www.sciencedirect.com/science/article/pii/S1388248108004748.

[19] Kati Miettunen, Imran Asghar, Simone Mastroianni, Janne Halme, Piers R.F. Barnes, Emma Rikkinen, Brian C. O'Regan, and Peter Lund.

Effect of molecular filtering and electrolyte composition on the spatial variation in performance of dye solar cells. *Journal of Electroanalytical Chemistry*, 664(Supplement C):63 – 72, 2012. ISSN 1572-6657. doi: https://doi.org/10.1016/j.jelechem.2011.10.012. URL http://www.sciencedirect.com/science/article/pii/S1572665711005303.

[20] Kati Miettunen, Piers R.F. Barnes, Xiaoe Li, ChunHung Law, and Brian C. O'Regan. The effect of electrolyte filling method on the performance of dye-sensitized solar cells. *Journal of Electroanalytical Chemistry*, 677(Supplement C):41 – 49, 2012. ISSN 1572-6657. doi: https://doi.org/10.1016/j.jelechem.2012.04.013. URL http://www.sciencedirect.com/science/article/pii/S1572665712001440.

[21] Syed Ghufran Hashmi, Kati Miettunen, Antti Ruuskanen, Imran Asghar, Janne Halme, and Peter Lund. Process steps towards a flexible dye solar cell module. *Proceedings of the 27th European Photovoltaic Solar Energy Conference*, 27, 2013. doi: 10.4229/27thEUPVSEC2012-3DV.4.42. URL http://dx.doi.org/10.4229/27thEUPVSEC2012-3DV.4.42.

[22] Guangda Niu, Xudong Guo, and Liduo Wang. Review of recent progress in chemical stability of perovskite solar cells. *J. Mater. Chem. A*, 3:8970–8980, 2015. doi: 10.1039/C4TA04994B. URL http://dx.doi.org/10.1039/C4TA04994B.

[23] Janne Halme, Paula Vahermaa, Kati Miettunen, and Peter Lund. Device physics of dye solar cells. *Advanced Materials*, 22(35):E210–E234, 2010. ISSN 1521-4095. doi: 10.1002/adma.201000726. URL http://dx.doi.org/10.1002/adma.201000726.

[24] Antonio Luque and Steven Hegedus. *Handbook of photovoltaic science and engineering*. John Wiley & Sons, 2011.

[25] Tetsuo Soga. *Nanostructured materials for solar energy conversion*. Elsevier, 2006.

[26] Anders Hagfeldt, Gerrit Boschloo, Licheng Sun, Lars Kloo, and Henrik Pettersson. Dye-sensitized solar cells. *Chemical Reviews*, 110(11):6595–6663, 2010. doi: 10.1021/cr900356p. URL http://dx.doi.org/10.1021/cr900356p. PMID: 20831177.

[27] Janne Halme, Gerrit Boschloo, Anders Hagfeldt, and Peter Lund. Spectral characteristics of light harvesting, electron injection, and steady-state charge collection in pressed tio2 dye solar cells. *The Journal of Physical Chemistry C*, 112(14):5623–5637, 2008. doi: 10.1021/jp711245f. URL http://dx.doi.org/10.1021/jp711245f.

[28] Akihiro Kojima, Kenjiro Teshima, Yasuo Shirai, and Tsutomu Miyasaka. Organometal halide perovskites as visible-light sensitizers for photovoltaic cells. *Journal of the American Chemical Society*, 131(17):6050–6051, 2009. doi: 10.1021/ja809598r. URL http://dx.doi.org/10.1021/ja809598r. PMID: 19366264.

[29] Hui-Seon Kim, Chang-Ryul Lee, Jeong-Hyeok Im, Ki-Beom Lee, Thomas Moehl, Arianna Marchioro, Soo-Jin Moon, Robin Humphry-Baker, Jun-Ho

Yum, Jacques E Moser, et al. Lead iodide perovskite sensitized all-solid-state submicron thin film mesoscopic solar cell with efficiency exceeding 9%. *Scientific reports*, 2, 2012. doi: 10.1038/srep00591.

[30] Michael M. Lee, Joël Teuscher, Tsutomu Miyasaka, Takurou N. Murakami, and Henry J. Snaith. Efficient hybrid solar cells based on meso-superstructured organometal halide perovskites. *Science*, 338(6107):643–647, 2012. ISSN 0036-8075. doi: 10.1126/science.1228604. URL http://science.sciencemag.org/content/338/6107/643.

[31] Surya Prakash Singh and P. Nagarjuna. Organometal halide perovskites as useful materials in sensitized solar cells. *Dalton Trans.*, 43:5247–5251, 2014. doi: 10.1039/C3DT53503G. URL http://dx.doi.org/10.1039/C3DT53503G.

[32] Taame Abraha Berhe, Wei-Nien Su, Ching-Hsiang Chen, Chun-Jern Pan, Ju-Hsiang Cheng, Hung-Ming Chen, Meng-Che Tsai, Liang-Yih Chen, Amare Aregahegn Dubale, and Bing-Joe Hwang. Organometal halide perovskite solar cells: degradation and stability. *Energy Environ. Sci.*, 9:323–356, 2016. doi: 10.1039/C5EE02733K. URL http://dx.doi.org/10.1039/C5EE02733K.

[33] Woon Seok Yang, Byung-Wook Park, Eui Hyuk Jung, Nam Joong Jeon, Young Chan Kim, Dong Uk Lee, Seong Sik Shin, Jangwon Seo, Eun Kyu Kim, Jun Hong Noh, and Sang Il Seok. Iodide management in formamidinium-lead-halide–based perovskite layers for efficient solar cells. *Science*, 356(6345):1376–1379, 2017. ISSN 0036-8075. doi: 10.1126/science.aan2301. URL http://science.sciencemag.org/content/356/6345/1376.

[34] Haining Chen and Shihe Yang. Carbon-based perovskite solar cells without hole transport materials: The front runner to the market? *Advanced Materials*, 29(24):1603994–n/a, 2017. ISSN 1521-4095. doi: 10.1002/adma.201603994. URL http://dx.doi.org/10.1002/adma.201603994. 1603994.

[35] Samuel D. Stranks, Giles E. Eperon, Giulia Grancini, Christopher Menelaou, Marcelo J. P. Alcocer, Tomas Leijtens, Laura M. Herz, Annamaria Petrozza, and Henry J. Snaith. Electron-hole diffusion lengths exceeding 1 micrometer in an organometal trihalide perovskite absorber. *Science*, 342(6156):341–344, 2013. ISSN 0036-8075. doi: 10.1126/science.1243982. URL http://science.sciencemag.org/content/342/6156/341.

[36] Lioz Etgar, Peng Gao, Zhaosheng Xue, Qin Peng, Aravind Kumar Chandiran, Bin Liu, Md. K. Nazeeruddin, and Michael Grätzel. Mesoscopic ch3nh3pbi3/tio2 heterojunction solar cells. *Journal of the American Chemical Society*, 134(42):17396–17399, 2012. doi: 10.1021/ja307789s. URL http://dx.doi.org/10.1021/ja307789s. PMID: 23043296.

[37] Zhiliang Ku, Yaoguang Rong, Mi Xu, Tongfa Liu, and Hongwei Han. Full printable processed mesoscopic ch3nh3pbi3/tio2 heterojunction solar cells with carbon counter electrode. *Scientific reports*, 3, 2013. doi: 10.1038/srep03132. URL http://dx.doi.org/10.1038/srep03132.

[38] Tomas Leijtens, Giles E. Eperon, Nakita K. Noel, Severin N. Habisreutinger, Annamaria Petrozza, and Henry J. Snaith. Stability of metal

halide perovskite solar cells. *Advanced Energy Materials*, 5(20):1500963–n/a, 2015. ISSN 1614-6840. doi: 10.1002/aenm.201500963. URL http://dx.doi.org/10.1002/aenm.201500963. 1500963.

[39] Yu Han, Steffen Meyer, Yasmina Dkhissi, Karl Weber, Jennifer M. Pringle, Udo Bach, Leone Spiccia, and Yi-Bing Cheng. Degradation observations of encapsulated planar ch3nh3pbi3 perovskite solar cells at high temperatures and humidity. *J. Mater. Chem. A*, 3:8139–8147, 2015. doi: 10.1039/C5TA00358J. URL http://dx.doi.org/10.1039/C5TA00358J.

[40] Dian Wang, Matthew Wright, Naveen Kumar Elumalai, and Ashraf Uddin. Stability of perovskite solar cells. *Solar Energy Materials and Solar Cells*, 147(Supplement C):255 – 275, 2016. ISSN 0927-0248. doi: https://doi.org/10.1016/j.solmat.2015.12.025. URL http://www.sciencedirect.com/science/article/pii/S092702481500673X.

[41] Anyi Mei, Xiong Li, Linfeng Liu, Zhiliang Ku, Tongfa Liu, Yaoguang Rong, Mi Xu, Min Hu, Jiangzhao Chen, Ying Yang, Michael Grätzel, and Hongwei Han. A hole-conductor–free, fully printable mesoscopic perovskite solar cell with high stability. *Science*, 345(6194):295–298, 2014. ISSN 0036-8075. doi: 10.1126/science.1254763. URL http://science.sciencemag.org/content/345/6194/295.

[42] Tongfa Liu, Linfeng Liu, Min Hu, Ying Yang, Lijun Zhang, Anyi Mei, and Hongwei Han. Critical parameters in tio2/zro2/carbon-based mesoscopic perovskite solar cell. *Journal of Power Sources*, 293(Supplement C): 533 – 538, 2015. ISSN 0378-7753. doi: https://doi.org/10.1016/j.jpowsour.2015.05.106. URL http://www.sciencedirect.com/science/article/pii/S0378775315010162.

[43] Jenny Nelson. *The physics of solar cells*. World Scientific Publishing Co Inc, 2003.

[44] Isaac Zarazua, Guifang Han, Pablo P. Boix, Subodh Mhaisalkar, Francisco Fabregat-Santiago, Ivan Mora-Seró, Juan Bisquert, and Germà Garcia-Belmonte. Surface recombination and collection efficiency in perovskite solar cells from impedance analysis. *The Journal of Physical Chemistry Letters*, 7(24):5105–5113, 2016. doi: 10.1021/acs.jpclett.6b02193. URL http://dx.doi.org/10.1021/acs.jpclett.6b02193. PMID: 27973858.

[45] L Murtomäki, T Kallio, R Lahtinen, and K Kontturi. Sähkökemia. *Teknillinen korkeakoulu*, 2010.

[46] Muhammad Imran Asghar, Kati Miettunen, Simone Mastroianni, Janne Halme, Henri Vahlman, and Peter Lund. In situ image processing method to investigate performance and stability of dye solar cells. *Solar Energy*, 86 (1):331 – 338, 2012. ISSN 0038-092X. doi: https://doi.org/10.1016/j.solener.2011.10.006. URL http://www.sciencedirect.com/science/article/pii/S0038092X11003732.

[47] Steven H Simon. *The Oxford solid state basics*. OUP Oxford, 2013.

[48] Harald Ibach and Hans Luth. *Solid-state physics: an introduction to theory and experiment*. Springer, 1993.

[49] Bernard Dennis Cullity and John W Weymouth. Elements of x-ray diffraction. *American Journal of Physics*, 25(6):394–395, 1957.

[50] Devinderjit Singh Sivia. *Elementary scattering theory: for X-ray and neutron users*. Oxford University Press, 2011.

[51] Takayuki Kitamura, Kenichi Okada, Hiroshi Matsui, and Nobuo Tanabe. Durability of dye-sensitized solar cells and modules. *Journal of Solar Energy Engineering*, 132(2):021105, 2010. doi: 10.1115/1.4001152. URL http://dx.doi.org/10.1115/1.4001152.

[52] J. M. Kroon, N. J. Bakker, H. J. P. Smit, P. Liska, K. R. Thampi, P. Wang, S. M. Zakeeruddin, M. Grätzel, A. Hinsch, S. Hore, U. Würfel, R. Sastrawan, J. R. Durrant, E. Palomares, H. Pettersson, T. Gruszecki, J. Walter, K. Skupien, and G. E. Tulloch. Nanocrystalline dye-sensitized solar cells having maximum performance. *Progress in Photovoltaics: Research and Applications*, 15(1):1–18, 2007. ISSN 1099-159X. doi: 10.1002/pip.707. URL http://dx.doi.org/10.1002/pip.707.

[53] D. Kuang, C. Klein, S. Ito, J.-E. Moser, R. Humphry-Baker, N. Evans, F. Duriaux, C. Grätzel, S.M. Zakeeruddin, and M. Grätzel. High-efficiency and stable mesoscopic dye-sensitized solar cells based on a high molar extinction coefficient ruthenium sensitizer and nonvolatile electrolyte. *Advanced Materials*, 19(8):1133–1137, 2007. ISSN 1521-4095. doi: 10.1002/adma.200602172. URL http://dx.doi.org/10.1002/adma.200602172.

[54] B. Macht, M. Turrión, A. Barkschat, P. Salvador, K. Ellmer, and H. Tributsch. Patterns of efficiency and degradation in dye sensitization solar cells measured with imaging techniques. *Solar Energy Materials and Solar Cells*, 73(2):163 – 173, 2002. ISSN 0927-0248. doi: https://doi.org/10.1016/S0927-0248(01)00121-0. URL http://www.sciencedirect.com/science/article/pii/S0927024801001210.

[55] Seigo Ito, Takurou N. Murakami, Pascal Comte, Paul Liska, Carole Grätzel, Mohammad K. Nazeeruddin, and Michael Grätzel. Fabrication of thin film dye sensitized solar cells with solar to electric power conversion efficiency over 10 *Thin Solid Films*, 516(14):4613 – 4619, 2008. ISSN 0040-6090. doi: https://doi.org/10.1016/j.tsf.2007.05.090. URL http://www.sciencedirect.com/science/article/pii/S0040609007009157. 6th International Conference on Coatings on Glass and Plastics (ICCG6)- Advanced Coatings for Large-Area or High-Volume Products-.

[56] Feng Hao, Hong Lin, Jing Zhang, Dongtian Zhuang, Yizhu Liu, and Jianbao Li. Influence of iodine concentration on the photoelectrochemical performance of dye-sensitized solar cells containing non-volatile electrolyte. *Electrochimica Acta*, 55(24):7225 – 7229, 2010. ISSN 0013-4686. doi: https://doi.org/10.1016/j.electacta.2010.06.079. URL http://www.sciencedirect.com/science/article/pii/S0013468610008959.

[57] Armi Tiihonen. The effect of electrolyte purification on performance and long-term stability of dye-sensitized solar cells. G2 pro gradu, diplomityö, 2013. URL http://urn.fi/URN:NBN:fi:aalto-201310307763.

[58] Katrine Flarup Jensen, Henning Brandt, Chan Im, Jürgen Wilde, and Andreas Hinsch. Stability of uv illuminated dye sensitized solar cells (dsc)

studied by photoinduced absorption in the second range. *PVSEC proceeding, Paris*, 2013, 2013. doi: 10.4229/28thEUPVSEC2013-3DV.2.27. URL http://dx.doi.org/10.4229/28thEUPVSEC2013-3DV.2.27.

[59] Matthew Carnie, Daniel Bryant, Trystan Watson, and David Worsley. Photocatalytic oxidation of triiodide in uva-exposed dye-sensitized solar cells. *International Journal of Photoenergy*, 2012, 2012. doi: 10.1155/2012/524590. URL http://dx.doi.org/10.1155/2012/524590.

[60] Matthew J. Carnie, Trystan Watson, D. T. Bryant, and David Worsley. Electrochemical characterization of the uv-photodegradation of dye-sensitized solar cells and usage in the assessment of uv-protection measures. *ECS Transactions*, 41(4):93–102, 2011. doi: 10.1149/1.3628613. URL http://ecst.ecsdl.org/content/41/4/93.abstract.

[61] Wei Guo, Liqiong Wu, Zhuo Chen, Gerrit Boschloo, Anders Hagfeldt, and Tingli Ma. Highly efficient dye-sensitized solar cells based on nitrogen-doped titania with excellent stability. *Journal of Photochemistry and Photobiology A: Chemistry*, 219(2):180 – 187, 2011. ISSN 1010-6030. doi: https://doi.org/10.1016/j.jphotochem.2011.01.004. URL http://www.sciencedirect.com/science/article/pii/S1010603011000074.

[62] Simone Mastroianni, Angelo Lembo, Thomas M. Brown, Andrea Reale, and Aldo Di Carlo. Electrochemistry in reverse biased dye solar cells and dye/electrolyte degradation mechanisms. *ChemPhysChem*, 13(12):2964–2975, 2012. ISSN 1439-7641. doi: 10.1002/cphc.201200229. URL http://dx.doi.org/10.1002/cphc.201200229.

[63] Tomas Leijtens, Giles E Eperon, Sandeep Pathak, Antonio Abate, Michael M Lee, and Henry J Snaith. Overcoming ultraviolet light instability of sensitized tio2 with meso-superstructured organometal tri-halide perovskite solar cells. *Nature communications*, 4:2885, 2013. doi: 10.1038/ncomms3885.

[64] Katrine Flarup Jensen, Welmoed Veurman, Henning Brandt, Chan Im, Jürgen Wilde, and Andreas Hinsch. Parameter study on uv-induced degradation of dye-sensitized solar cells. *MRS Online Proceedings Library Archive*, 1537, 2013. doi: 10.1557/opl.2013.790. URL https://doi.org/10.1557/opl.2013.790.

[65] Ravi Harikisun and Hans Desilvestro. Long-term stability of dye solar cells. *Solar Energy*, 85(6):1179 – 1188, 2011. ISSN 0038-092X. doi: https://doi.org/10.1016/j.solener.2010.10.016. URL http://www.sciencedirect.com/science/article/pii/S0038092X10003221. Organic photovoltaics and dye sensitized solar cells.

[66] Aswani Yella, Hsuan-Wei Lee, Hoi Nok Tsao, Chenyi Yi, Aravind Kumar Chandiran, Md.Khaja Nazeeruddin, Eric Wei-Guang Diau, Chen-Yu Yeh, Shaik M Zakeeruddin, and Michael Grätzel. Porphyrin-sensitized solar cells with cobalt (ii/iii)–based redox electrolyte exceed 12 percent efficiency. *Science*, 334(6056):629–634, 2011. ISSN 0036-8075. doi: 10.1126/science.1209688. URL http://science.sciencemag.org/content/334/6056/629.

[67] Zhe Sun, Mao Liang, and Jun Chen. Kinetics of iodine-free redox shuttles in dye-sensitized solar cells: Interfacial recombination and dye regeneration. *Accounts of Chemical Research*, 48(6):1541–1550, 2015. doi:

10.1021/ar500337g. URL http://dx.doi.org/10.1021/ar500337g. PMID: 26001106.

[68] Kati Miettunen, Tapio Saukkonen, Xiaoe Li, ChunHung Law, Yeo Kee Sheng, Janne Halme, Armi Tiihonen, Piers R. F. Barnes, Tarek Ghaddar, Imran Asghar, Peter Lund, and Brian C. O'Regan. Do counter electrodes on metal substrates work with cobalt complex based electrolyte in dye sensitized solar cells? *Journal of The Electrochemical Society*, 160(2): H132–H137, 2013. doi: 10.1149/2.074302jes. URL http://jes.ecsdl.org/content/160/2/H132.abstract.

[69] Kati Miettunen, Sami Jouttijärvi, Roger Jiang, Tapio Saukkonen, Jyrki Romu, Janne Halme, and Peter Lund. Low cost ferritic stainless steel in dye sensitized solar cells with cobalt complex electrolyte. *Journal of The Electrochemical Society*, 161(3):H138–H143, 2014. doi: 10.1149/2.054403jes. URL http://jes.ecsdl.org/content/161/3/H138.abstract.

[70] Jiajia Gao, Muthuraaman Bhagavathi Achari, and Lars Kloo. Long-term stability for cobalt-based dye-sensitized solar cells obtained by electrolyte optimization. *Chem. Commun.*, 50:6249–6251, 2014. doi: 10.1039/C4CC00698D. URL http://dx.doi.org/10.1039/C4CC00698D.

[71] Roger Jiang, Assaf Anderson, Piers R. F. Barnes, Li Xiaoe, Chunhung Law, and Brian C. O'Regan. 2000 hours photostability testing of dye sensitised solar cells using a cobalt bipyridine electrolyte. *J. Mater. Chem. A*, 2:4751–4757, 2014. doi: 10.1039/C4TA00402G. URL http://dx.doi.org/10.1039/C4TA00402G.

[72] Federico Bella, Simone Galliano, Claudio Gerbaldi, and Guido Viscardi. Cobalt-based electrolytes for dye-sensitized solar cells: Recent advances towards stable devices. *Energies*, 9(5), 2016. ISSN 1996-1073. doi: 10.3390/en9050384. URL http://www.mdpi.com/1996-1073/9/5/384.

[73] Sabine M. K. Rendon, Denys Mavrynsky, Axel Meierjohann, Armi Tiihonen, Kati Miettunen, Imran Asghar, Janne Halme, Leif Kronberg, and Reko Leino. Analysis of dye degradation products and assessment of the dye purity in dye-sensitized solar cells. *Rapid Communications in Mass Spectrometry*, 29(23):2245–2251, 2015. ISSN 1097-0231. doi: 10.1002/rcm.7384. URL http://dx.doi.org/10.1002/rcm.7384. RCM-15-0198.R1.

[74] Wanchun Xiang, Wenchao Huang, Udo Bach, and Leone Spiccia. Stable high efficiency dye-sensitized solar cells based on a cobalt polymer gel electrolyte. *Chem. Commun.*, 49:8997–8999, 2013. doi: 10.1039/C3CC44555K. URL http://dx.doi.org/10.1039/C3CC44555K.

[75] Naohiko Kato, Yasuhiko Takeda, Kazuo Higuchi, Akihiro Takeichi, Eiichi Sudo, Hiromitsu Tanaka, Tomoyoshi Motohiro, Toshiyuki Sano, and Tatsuo Toyoda. Degradation analysis of dye-sensitized solar cell module after long-term stability test under outdoor working condition. *Solar Energy Materials and Solar Cells*, 93(6):893 – 897, 2009. ISSN 0927-0248. doi: https://doi.org/10.1016/j.solmat.2008.10.022. URL http://www.sciencedirect.com/science/article/pii/S0927024808003644. 17th International Photovoltaic Science and Engineering Conference.

[76] S. Schuller, P. Schilinsky, J. Hauch, and C.J. Brabec. Determination of the degradation constant of bulk heterojunction solar cells by accelerated lifetime measurements. *Applied Physics A*, 79(1):37–40, Jun 2004. ISSN 1432-0630. doi: 10.1007/s00339-003-2499-4. URL https://doi.org/10.1007/s00339-003-2499-4.

[77] Rémi De Bettignies, Jocelyne Leroy, Muriel Firon, and Carole Sentein. Accelerated lifetime measurements of p3ht:pcbm solar cells. *Synthetic Metals*, 156(7):510 – 513, 2006. ISSN 0379-6779. doi: https://doi.org/10.1016/j.synthmet.2005.06.016. URL http://www.sciencedirect.com/science/article/pii/S0379677905007320.

[78] Kai Zhu, Nathan R. Neale, Alexander Miedaner, and Arthur J. Frank. Enhanced charge-collection efficiencies and light scattering in dye-sensitized solar cells using oriented tio2 nanotubes arrays. *Nano Letters*, 7(1):69–74, 2007. doi: 10.1021/nl062000o. URL http://dx.doi.org/10.1021/nl062000o. PMID: 17212442.

[79] Ze Yu, Mikhail Gorlov, Jarl Nissfolk, Gerrit Boschloo, and Lars Kloo. Investigation of iodine concentration effects in electrolytes for dye-sensitized solar cells. *The Journal of Physical Chemistry C*, 114(23):10612–10620, 2010. doi: 10.1021/jp1001918. URL http://dx.doi.org/10.1021/jp1001918.

[80] Marcos A.S. Andrade, Ana F. Nogueira, Kati Miettunen, Armi Tiihonen, Peter D. Lund, and Heloise O. Pastore. Quasi-solid electrolyte with polyamidoamine dendron modified-talc applied to dye-sensitized solar cells. *Journal of Power Sources*, 325(Supplement C):161 – 170, 2016. ISSN 0378-7753. doi: https://doi.org/10.1016/j.jpowsour.2016.06.041. URL http://www.sciencedirect.com/science/article/pii/S0378775316307431.

[81] Marcos A. Santana Andrade, Armi Tiihonen, Kati Miettunen, Peter Lund, Ana F. Nogueira, and Heloise O. Pastore. Gel electrolytes with polyamidopyridine dendron modified talc for dye-sensitized solar cells. *ACS Applied Materials & Interfaces*, 9(24):20454–20466, 2017. doi: 10.1021/acsami.7b00897. URL http://dx.doi.org/10.1021/acsami.7b00897. PMID: 28574246.

[82] Marcos A. Santana Andrade, Kati Miettunen, Armi Tiihonen, Peter D. Lund, Ana F. Nogueira, and Heloise O. Pastore. Stabilizing dendron-modified talc-based electrolyte for quasi-solid dye-sensitized solar cell. *Electrochimica Acta*, 228(Supplement C):413 – 421, 2017. ISSN 0013-4686. doi: https://doi.org/10.1016/j.electacta.2017.01.101. URL http://www.sciencedirect.com/science/article/pii/S0013468617301275.

[83] Gabriela G. Sonai, Armi Tiihonen, Kati Miettunen, Peter D. Lund, and Ana F. Nogueira. Long-term stability of dye-sensitized solar cells assembled with cobalt polymer gel electrolyte. *The Journal of Physical Chemistry C*, 121(33):17577–17585, 2017. doi: 10.1021/acs.jpcc.7b03865. URL http://dx.doi.org/10.1021/acs.jpcc.7b03865.

[84] Marjo Pääkkö, Jaana Vapaavuori, Riitta Silvennoinen, Harri Kosonen, Mikael Ankerfors, Tom Lindström, Lars A. Berglund, and Olli Ikkala. Long and entangled native cellulose i nanofibers allow flexible aerogels and hierarchically porous templates for functionalities. *Soft Matter*, 4:2492–2499, 2008. doi: 10.1039/B810371B. URL http://dx.doi.org/10.1039/B810371B.

[85] Linfeng Liu, Anyi Mei, Tongfa Liu, Pei Jiang, Yusong Sheng, Lijun Zhang, and Hongwei Han. Fully printable mesoscopic perovskite solar cells with organic silane self-assembled monolayer. *Journal of the American Chemical Society*, 137(5):1790–1793, 2015. doi: 10.1021/ja5125594. URL http://dx.doi.org/10.1021/ja5125594. PMID: 25594109.

[86] Jiangzhao Chen, Yaoguang Rong, Anyi Mei, Yuli Xiong, Tongfa Liu, Yusong Sheng, Pei Jiang, Li Hong, Yanjun Guan, Xiaotong Zhu, Xiaomeng Hou, Miao Duan, Jianquan Zhao, Xiong Li, and Hongwei Han. Hole-conductor-free fully printable mesoscopic solar cell with mixed-anion perovskite ch3nh3pbi(3-x)(bf4)x. *Advanced Energy Materials*, 6(5):1502009–n/a, 2016. ISSN 1614-6840. doi: 10.1002/aenm.201502009. URL http://dx.doi.org/10.1002/aenm.201502009. 1502009.

[87] Huawei Zhou, Yantao Shi, Qingshun Dong, Hong Zhang, Yujin Xing, Kai Wang, Yi Du, and Tingli Ma. Hole-conductor-free, metal-electrode-free tio2/ch3nh3pbi3 heterojunction solar cells based on a low-temperature carbon electrode. *The Journal of Physical Chemistry Letters*, 5(18):3241–3246, 2014. doi: 10.1021/jz5017069. URL http://dx.doi.org/10.1021/jz5017069. PMID: 26276339.

[88] Dainius Perednis and Ludwig J. Gauckler. Thin film deposition using spray pyrolysis. *Journal of Electroceramics*, 14(2):103–111, Mar 2005. ISSN 1573-8663. doi: 10.1007/s10832-005-0870-x. URL https://doi.org/10.1007/s10832-005-0870-x.

[89] Shao-Gang Li, Ke-Jian Jiang, Mei-Ju Su, Xue-Ping Cui, Jin-Hua Huang, Qian-Qian Zhang, Xue-Qin Zhou, Lian-Min Yang, and Yan-Lin Song. Inkjet printing of ch3nh3pbi3 on a mesoscopic tio2 film for highly efficient perovskite solar cells. *J. Mater. Chem. A*, 3:9092–9097, 2015. doi: 10.1039/C4TA05675B. URL http://dx.doi.org/10.1039/C4TA05675B.

[90] Monojit Bag, Ziwen Jiang, Lawrence A. Renna, Seung Pyo Jeong, Vincent M. Rotello, and D. Venkataraman. Rapid combinatorial screening of inkjet-printed alkyl-ammonium cations in perovskite solar cells. *Materials Letters*, 164:472 – 475, 2016. ISSN 0167-577X. doi: https://doi.org/10.1016/j.matlet.2015.11.058. URL https://www.sciencedirect.com/science/article/pii/S0167577X1530879X.

[91] Zhanhua Wei, Haining Chen, Keyou Yan, and Shihe Yang. Inkjet printing and instant chemical transformation of a ch3nh3pbi3/nanocarbon electrode and interface for planar perovskite solar cells. *Angewandte Chemie*, 126 (48):13455–13459, 2014. ISSN 1521-3757. doi: 10.1002/ange.201408638. URL http://dx.doi.org/10.1002/ange.201408638.

[92] M. D. Kempe. Accelerated uv test methods and selection criteria for encapsulants of photovoltaic modules. In *2008 33rd IEEE Photovoltaic Specialists Conference*, pages 1–6, May 2008. doi: 10.1109/PVSC.2008.4922771.

[93] Yang Yang and Jingbi You. Make perovskite solar cells stable. *Nature*, 544 (7649):155–156, 2017. doi: 10.1038/544155a. URL http://dx.doi.org/10.1038/544155a.

[94] Editorial. A checklist for photovoltaic research. *Nature Materials*, 14(11): 1073, 2015. doi: 10.1038/nmat4473. URL http://dx.doi.org/10.1038/nmat4473.

[95] Qi Dong, Fangzhou Liu, Man Kwong Wong, Ho Won Tam, Aleksandra B. Djurišić, Annie Ng, Charles Surya, Wai Kin Chan, and Alan Man Ching Ng. Encapsulation of perovskite solar cells for high humidity conditions. *ChemSusChem*, 9(18):2597–2603, 2016. ISSN 1864-564X. doi: 10.1002/cssc.201600868. URL http://dx.doi.org/10.1002/cssc.201600868.

[96] T. Ibn-Mohammed, S.C.L. Koh, I.M. Reaney, A. Acquaye, G. Schileo, K.B. Mustapha, and R. Greenough. Perovskite solar cells: An integrated hybrid lifecycle assessment and review in comparison with other photovoltaic technologies. *Renewable and Sustainable Energy Reviews*, 80(Supplement C):1321 – 1344, 2017. ISSN 1364-0321. doi: https://doi.org/10.1016/j.rser.2017.05.095. URL http://www.sciencedirect.com/science/article/pii/S1364032117307311.

Aalto-DD 41/2018

ISBN 978-952-60-7879-3 (printed)
ISBN 978-952-60-7880-9 (pdf)
ISSN-L 1799-4934
ISSN 1799-4934 (printed)
ISSN 1799-4942 (pdf)

Aalto University
School of Science
Department of Applied physics
www.aalto.fi

BUSINESS + ECONOMY

ART + DESIGN + ARCHITECTURE

SCIENCE + TECHNOLOGY

CROSSOVER

DOCTORAL DISSERTATIONS